Cretaceous Research (2001) **22,** 173–199
doi:10.1006/cres.2001.0248, available online at http://www.idealibrary.com on IDEAL®

The Aptian, Albian and Cenomanian of Roter Sattel, Romandes Prealps, Switzerland: a high-resolution record of oceanographic changes

André Strasser, Michèle Caron and Maksim Gjermeni

Institut de Géologie, Université de Fribourg, Pérolles, 1700 Fribourg, Switzerland

Revised manuscript accepted 3 January 2001

The Aptian–Lower Turonian hemipelagic sediments of Roter Sattel in the Swiss Prealps are well dated by planktonic foraminifera. Stacking pattern of the limestone-marl alternations and facies evolution allow the identification of sequence boundaries, transgressive surfaces, and maximum-flooding events or condensed sections on at least two hierarchical levels. Calibrated by a precise biostratigraphic framework, the major sequence boundaries can be correlated with those recognized elsewhere in European basins. Organic-rich black shales are generally confined to transgressive and/or condensed intervals and correspond to the oceanic anoxic events (OAE) 1a–d and 2. OAE 1a and OAE 2 show well-marked positive shifts in $\delta^{13}C$. High-resolution analysis of the Roter Sattel section shows that eustatic sea-level changes and fluctuations in the global carbon cycle are clearly recognizable. However, these were overprinted by regional changes of climate and availability of terrigenous source areas controlling nutrient input and hence organic productivity, and by regional and local tectonics shaping basin morphology and modifying the paths of oceanic currents. This led to facies changes, strongly varying sedimentation rates, and non-deposition or erosion during the Aptian *Planomalina cheniourensis* Zone. Despite this distortion of the sedimentary record, the Roter Sattel section may serve as a corner-stone for the study of basin-wide or global oceanographic, climatic, and evolutionary changes when correlated with sections in other palaeogeographical domains.

KEY WORDS: Aptian; Albian; Cenomanian; planktonic foraminifera; black shales; oceanic anoxic events; sequence stratigraphy; Swiss Prealps.

1. Introduction

The Roter Sattel section discussed here is exceptional in that it offers a continuous exposure of Barremian–Turonian sediments deposited in the Briançonnais Domain, a complexly structured belt along the northern margin of the Alpine Tethys Ocean. Throughout its sedimentary history from the Triassic to the Eocene this domain has been affected by extensional and compressional tectonics, creating a patchwork of shallow platforms and deeper basins (Mettraux & Mosar, 1989; Hable, 1997). The Briançonnais has been interpreted as a terrane that separated from the Iberian continental margin in the Late Jurassic, which then drifted eastward and eventually formed a swell isolating the Valais Trough from the Liguro-Piemontese Ocean (Stampfli, 1993). Thrusting of the Briançonnais Domain took place during the early Tertiary, and its sedimentary cover now comprises an important part of the nappes of the Romandes and Chablais Prealps (e.g., Caron, 1973; Trümpy, 1980). The tectonic unit in which the Roter Sattel section is situated belongs to the Préalpes Médianes Plastiques. Palaeogeographically, it originated from the Subbriançonnais Zone between the Briançonnais High and the deeper depositional environments of the Valais Trough (Baud & Septfontaine, 1980).

Despite this regionally differentiated palaeogeographic and tectonic framework, globally recognized eustatic sea-level changes and oceanic anoxic events are recorded in the section studied. The aim of this paper is to give a detailed description of this sedimentary record and to interpret its evolution through time. Precise biochronostratigraphic dating enables the correlation of depositional sequences with the sequence-stratigraphic chart of Hardenbol *et al.* (1998), and the identification of intervals corresponding to oceanic anoxic events. This correlation then provides a basis for discussing the respective roles of tectonics,

0195–6671/01/020173+27 $35.00/0

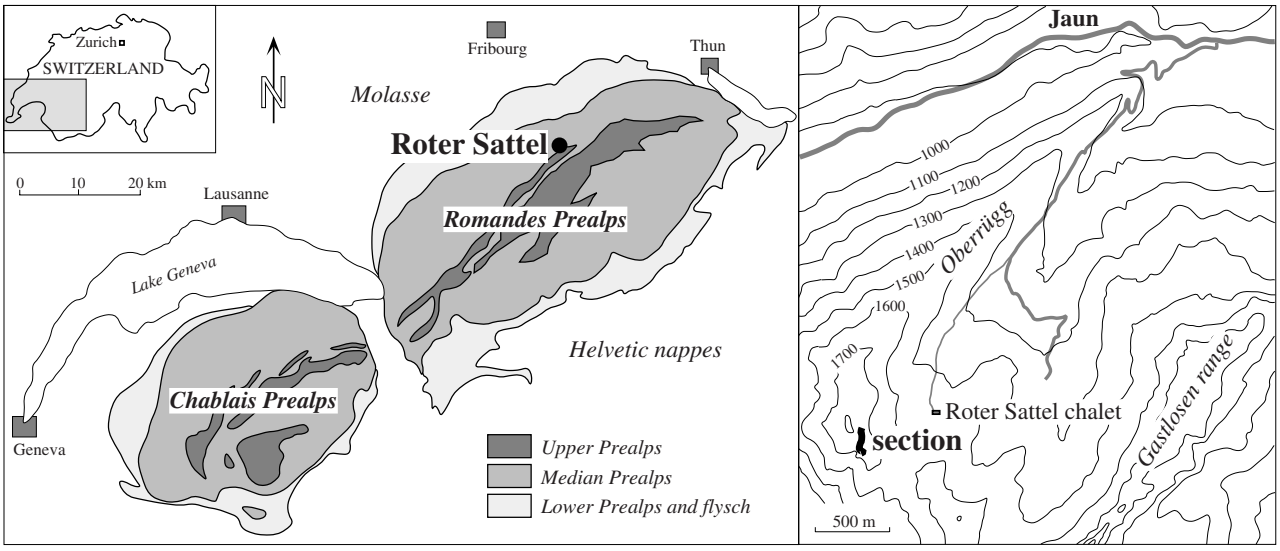

Figure 1. Location map of Roter Sattel outcrop in the Median Prealps of southwestern Switzerland.

sea level, and ocean circulation in controlling the depositional environments.

2. Description of the outcrop

The section studied is situated to the WSW of the chalet called Roter Sattel, which takes its name from the reddish lithologies of the Upper Cretaceous–lower Tertiary Couches Rouges, which crop out on the nearby mountain pass. The measured section starts at the base of the cliffs at point 585900/159440 (Swiss coordinates, sheet 1226 Boltigen of the 1:25,000 topographical map), at an altitude of 1700 m (Figure 1). The section then runs southwards along the base of the cliffs, crossing the three gullies formed by the erosion of softer, marly lithologies (Figure 2). The exposure is continuous and only weakly disturbed by small-scale tectonic faults. It ends at point 585950/159350. The general dip is about 75° to the SE.

The exposure was first described, as the Oberrügg section, by Page (1969) who dated it using planktonic foraminifera. Python-Dupasquier (1990) then provided a detailed log and used it as the type locality of the Intyamon Formation, spanning the interval from Lower Aptian to Middle Turonian. The underlying Calcaires-Plaquetés Formation is of Barremian age; the overlying Couches-Rouges Group encompasses the Upper Turonian–Lower Eocene. The Intyamon Formation is further subdivided into the Combe d'Avau (Lower Aptian–Upper Albian) and Chällihorn (Lower Cenomanian–Middle Turonian) members (Python-Dupasquier, 1990).

Building on this previous work we measured the 68-m-long section bed by bed and took 361 samples (Figure 3a–h). The biostratigraphic zonation has been established with great precision, and the facies and sequential evolution monitored in considerable detail.

3. Lithology, microfacies, and organic matter

Three major lithologies occur in the section studied: limestones, marls, and black shales. Variations within each lithology, however, can be important.

3.1. Limestones

Limestone beds are from a few cm to a few tens of cm thick (Figure 4a). They are light grey, beige, or reddish on the weathered surfaces but dark grey to black when freshly broken. They are commonly bioturbated and contain *Zoophycos*, *Planolites*, and *Chondrites*, a trace-fossil assemblage that points to outer-shelf to slope depositional environments and variable oxygenation (e.g., Jordan, 1985). Small pyrite cubes occur locally and indicate anoxic micro-environments, possibly owing to bacterial decomposition of organic matter. Some limestone beds contain chert nodules or layers.

Under the microscope, textures are seen to vary from mudstone to wackestone and packstone. Grainstones occur in some intervals and indicate winnowing by bottom currents. Planktonic foraminifera (Figure 5a) are present to abundant in almost all samples. Radiolarians (Figure 5b) are present to abundant in

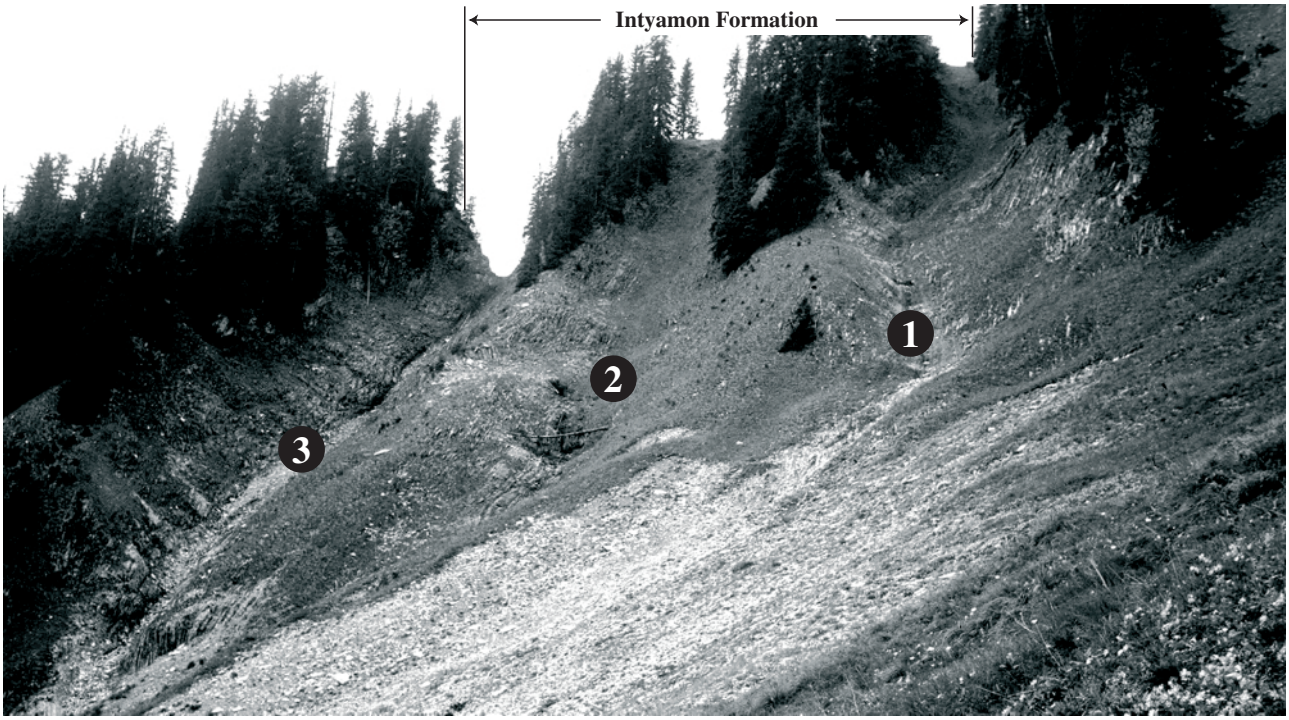

Figure 2. General view of exposure studied, looking WSW from the chalet Roter Sattel. Numbers indicate first, second, and third black-shale intervals.

certain intervals and absent from others. Marly intervals and siliceous limestones generally are richer in radiolarians, whereas limestone-dominated intervals contain more planktonic foraminifera (Figure 3). Calcispheres, sponge spicules, benthic foraminifera and bivalves, inoceram prisms, echinoderms, and peloids occur sporadically but never in great quantities. Small grains of phosphate and glauconite are found throughout the section. Detrital quartz grains occur preferentially in limestone beds of black-shale-dominated intervals (Figure 3), and are commonly overgrown by authigenic quartz. Small pyrite crystals are dispersed in the matrix, or concentrated in patches. Lithoclasts and reworked calpionellids (Figure 5c) appear preferentially in limestones of black-shale-dominated intervals and indicate erosion of pre-existing, more or less consolidated sediment.

Under the scanning electron microscope (SEM) it becomes evident that a large part of the carbonate matrix is composed of nannofossils (Figure 5d). The limestone beds can, therefore, be interpreted to have formed mostly through productivity cycles of nannoflora and planktonic foraminifera, with only a small part of the carbonate having been furnished from shallower environments or from erosion on the slope. However, many limestone beds show thin (mm) laminations composed of plankton-poor and plankton-rich layers, the latter locally forming grainstones (Figure 5e). This may indicate the action of contour currents that periodically winnowed the sea floor (Stow, 1994). Laminated and graded beds a few centimetres thick occur in some intervals and are interpreted as distal turbidites. Higher-energy conditions are also indicated by irregular, downcutting bedding surfaces as a result of scouring, and by convex-up beds that are interpreted to have been shaped by bottom currents or storm waves.

Neither planktonic foraminifera nor radiolarians are deformed (Figure 5f): their voids have been filled by calcite or chalcedony during early diagenesis and resisted post-depositional compaction. Primary sedimentary structures were, therefore, preserved.

Figure 3. Detailed log of lowermost Aptian–lowermost Turonian sediments at Roter Sattel. The sedimentary column represents the field aspect. The grey scale has been chosen according to the field observations but, of course, is highly subjective. Radiolarians (black bars) and planktonic foraminifera (white bars) are shown in relative abundances, the sum being 100%. Sequence boundaries Ap 2–Ce 5 are labelled according to Hardenbol *et al.* (1998).

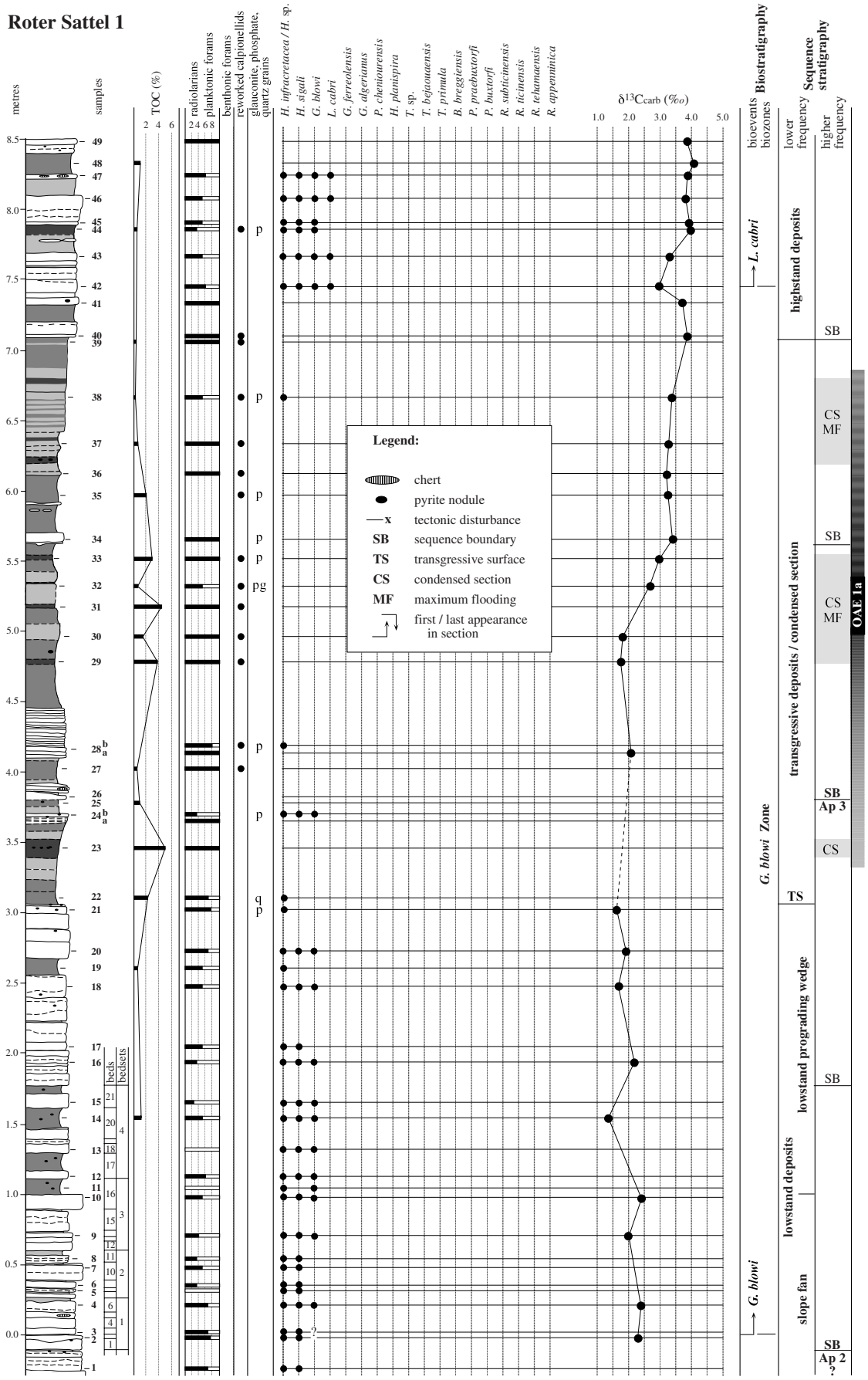
Roter Sattel 1
metres
samples
TOC (%)
radiolarians
planktonic forams
benthonic forams
reworked calpionellids
glauconite, phosphate, quartz grains
H. infracretacea / H. sp.
H. sigali
G. blowi
L. cabri
G. ferreolensis
G. algerianus
P. cheniourensis
H. planispira
T. sp.
T. bejaouaensis
T. primula
B. breggiensis
P. praebuxtorfi
P. buxtorfi
R. subticinensis
R. ticinensis
R. tehamaensis
R. appenninica
δ13Ccarb (‰)
Biostratigraphy
bioevents
biozones
Sequence stratigraphy
lower frequency
higher frequency
highstand deposits
transgressive deposits / condensed section
lowstand prograding wedge
lowstand deposits
slope fan
L. cabri
G. blowi Zone
G. blowi
SB
CS
MF
TS
Ap 3
Ap 2
OAE 1a
beds
bedsets
Legend:
chert
pyrite nodule
tectonic disturbance
sequence boundary
transgressive surface
condensed section
maximum flooding
first / last appearance in section

Figure 3 (a)

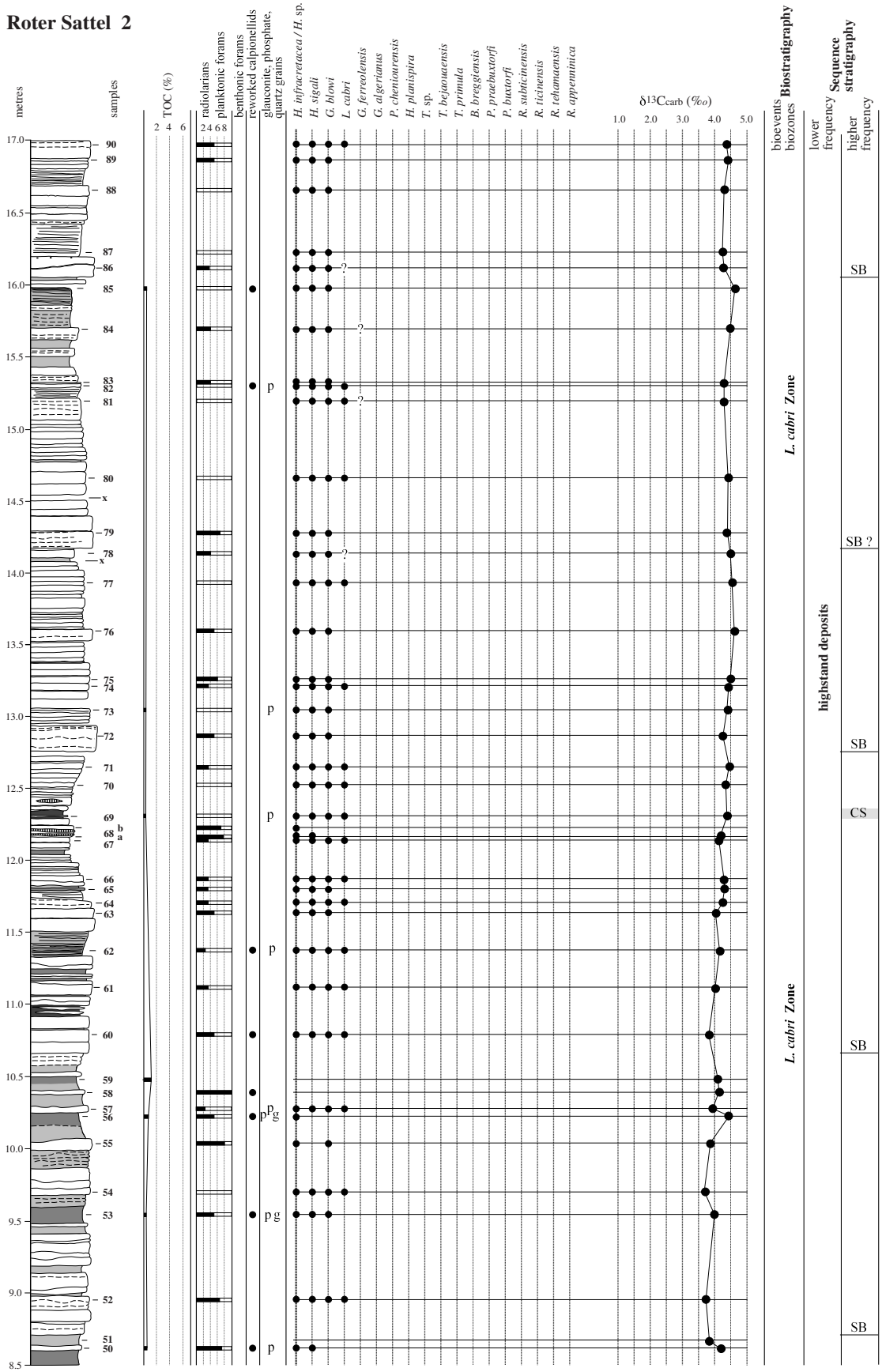
Roter Sattel 2
metres
samples
TOC (%)
radiolarians
planktonic forams
benthonic forams
reworked calpionellids
glauconite, phosphate, quartz grains
H. infracretacea / H. sp.
H. sigali
G. blowi
L. cabri
G. ferreolensis
G. algerianus
P. cheniourensis
H. planispira
T. sp.
T. bejaouaensis
T. primula
B. breggiensis
P. praebuxtorfi
P. buxtorfi
R. subticinensis
R. ticinensis
R. rehanaensis
R. appenninica
δ13Ccarb (‰)
bioevents
biozones
Biostratigraphy
lower frequency
Sequence stratigraphy
higher frequency
L. cabri Zone
highstand deposits
SB
SB ?
CS

Figure 3 (b)

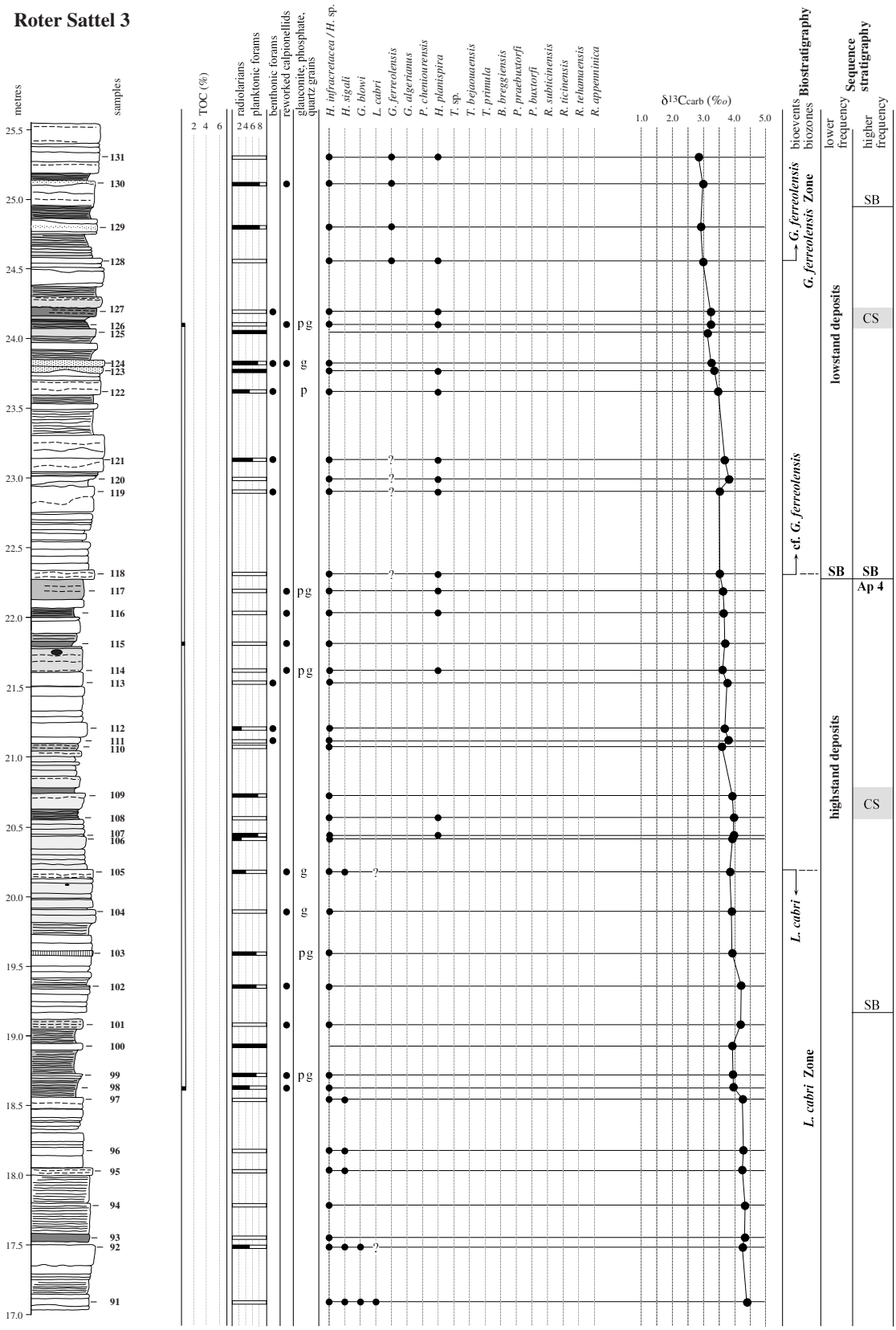
Roter Sattel 3
metres
samples
TOC (%)
radiolarians
planktonic forams
benthonic forams
reworked calpionellids
glauconite, phosphate, quartz grains
H. infracretacea / H. sp.
H. sigali
G. blowi
L. cabri
G. ferreolensis
G. algerianus
P. cheniouensis
H. planispira
T. sp.
T. bejaouaensis
T. primula
B. breggiensis
P. praebuxtorfi
P. buxtorfi
R. subticinensis
R. ticinensis
R. tehamaensis
R. appeninica
δ13Ccarb (‰)
Biostratigraphy
biozones
Sequence stratigraphy
lower frequency
higher frequency
G. ferreolensis Zone
cf. G. ferreolensis
L. cabri Zone
lowstand deposits
highstand deposits
SB
CS
Ap 4

Figure 3 (c)

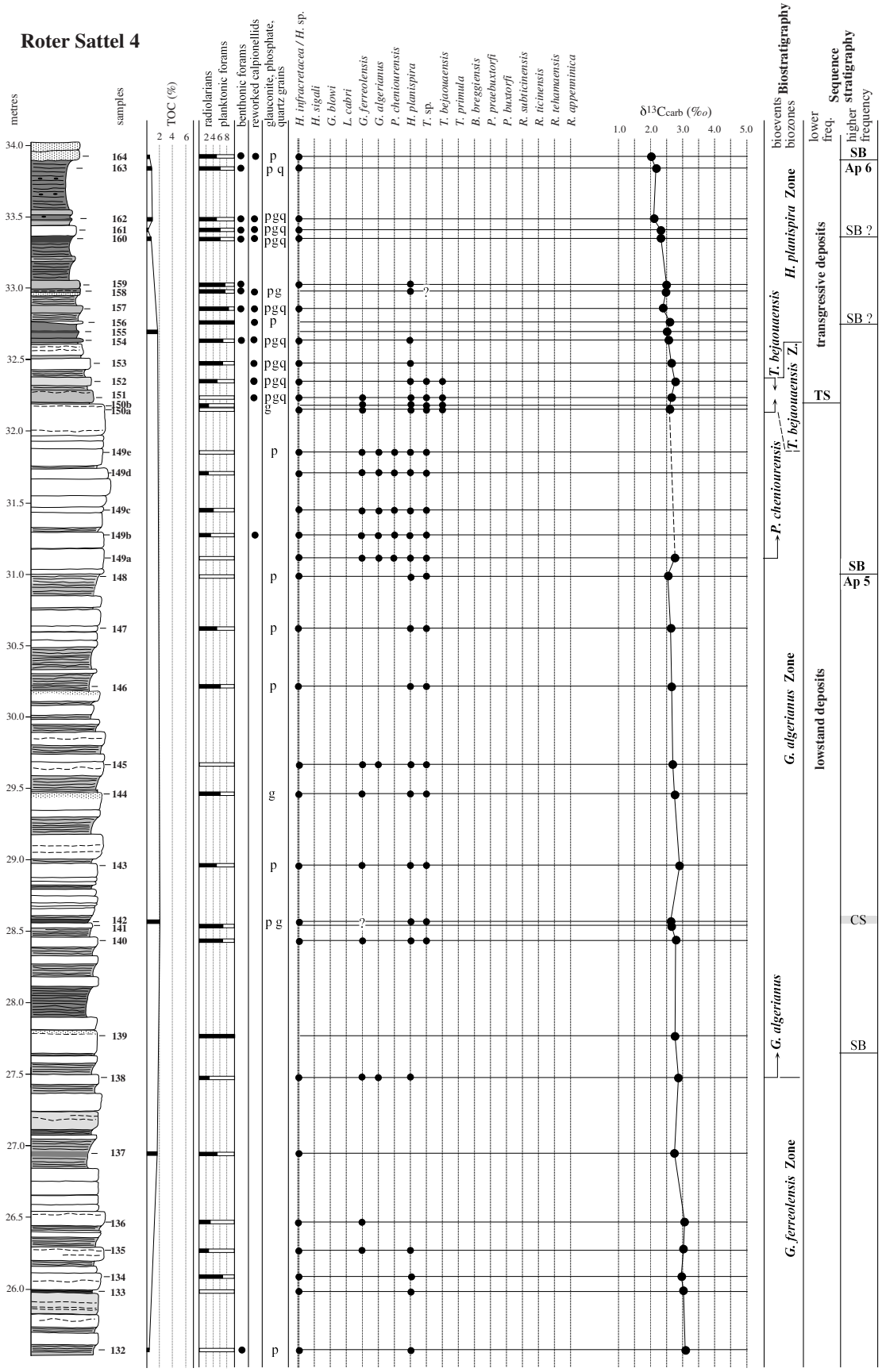
Roter Sattel 4
metres
samples
TOC (%)
radiolarians
planktonic forams
benthonic forams
reworked calpionellids
glauconite, phosphate, quartz grains
H. infracretacea / H. sp.
H. sigali
G. blowi
L. cabri
G. ferreolensis
G. algerianus
P. cheniourensis
H. planispira
T. sp.
T. bejaouaensis
T. primula
B. breggiensis
P. praebuxtorfi
P. buxtorfi
R. subticinensis
R. ticinensis
R. tehamaensis
R. apenninica
δ13Ccarb (‰)
bioevents
biozones
Biostratigraphy
lower freq.
higher frequency
Sequence stratigraphy
H. planispira Zone
T. bejaouaensis Z.
P. cheniourensis
G. algerianus Zone
G. algerianus
G. ferreolensis Zone
transgressive deposits
lowstand deposits
TS
SB
Ap 6
SB ?
SB ?
SB
Ap 5
CS
SB

Figure 3 (d)

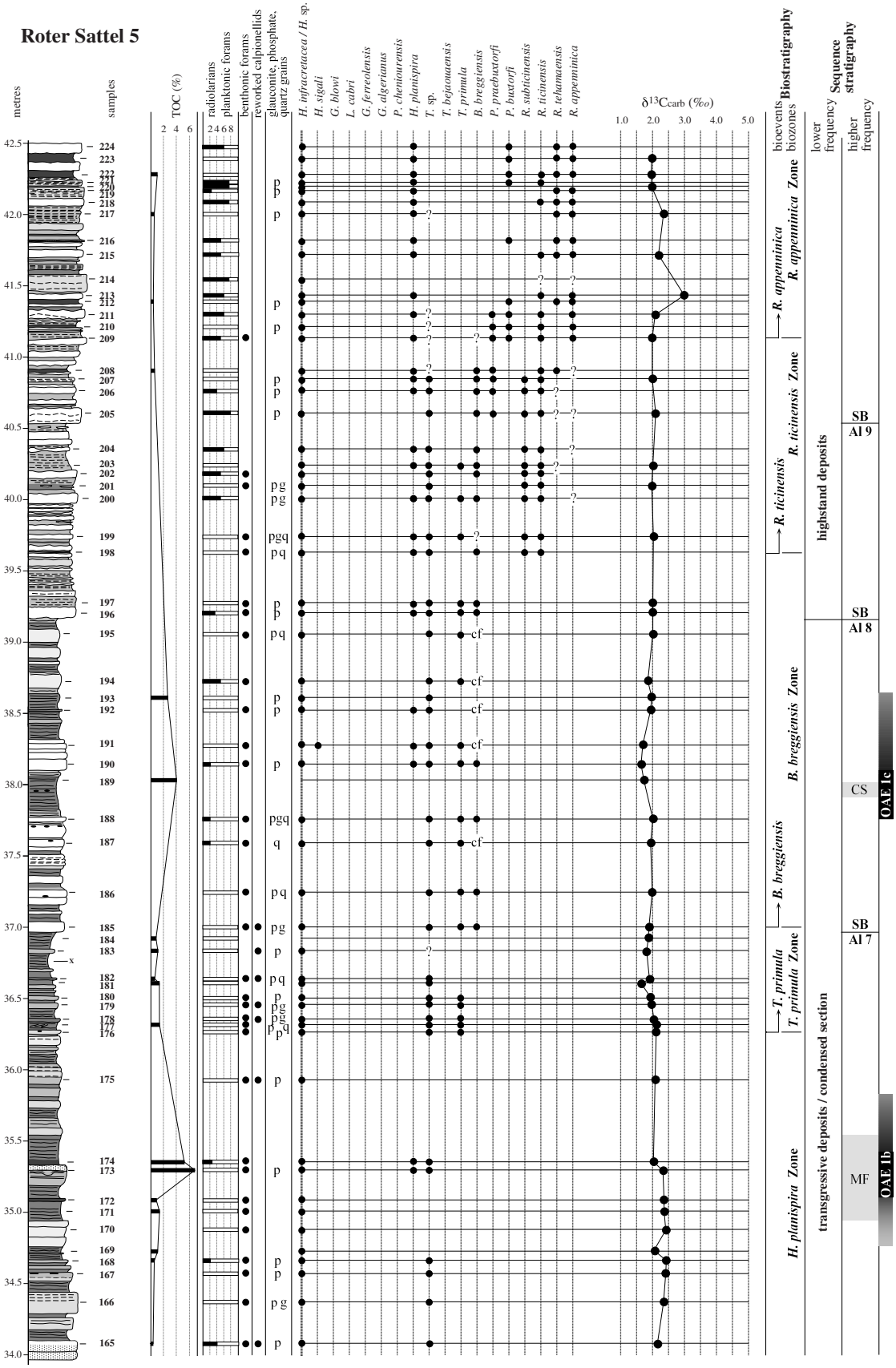
Roter Sattel 5
metres
samples
TOC (%)
radiolarians
planktonic forams
benthonic forams
reworked calpionellids
glauconite, phosphate, quartz grains
H. infracretacea / H. sp.
H. sigali
G. blowi
L. cabri
G. ferreolensis
G. algerianus
P. chenionensis
H. planispira
T. sp.
T. bejaouaensis
T. primula
B. breggiensis
P. praebuxtorfi
P. buxtorfi
R. subticinensis
R. ticinensis
R. tethamensis
R. appenninica
δ13Ccarb (‰)
Biostratigraphy
bioevents
biozones
Sequence stratigraphy
lower frequency
higher frequency
R. appenninica Zone
R. ticinensis Zone
B. breggiensis Zone
T. primula Zone
H. planispira Zone
highstand deposits
transgressive deposits / condensed section
SB
AI 9
AI 8
AI 7
CS
MF
OAE 1c
OAE 1b

Figure 3 (e)

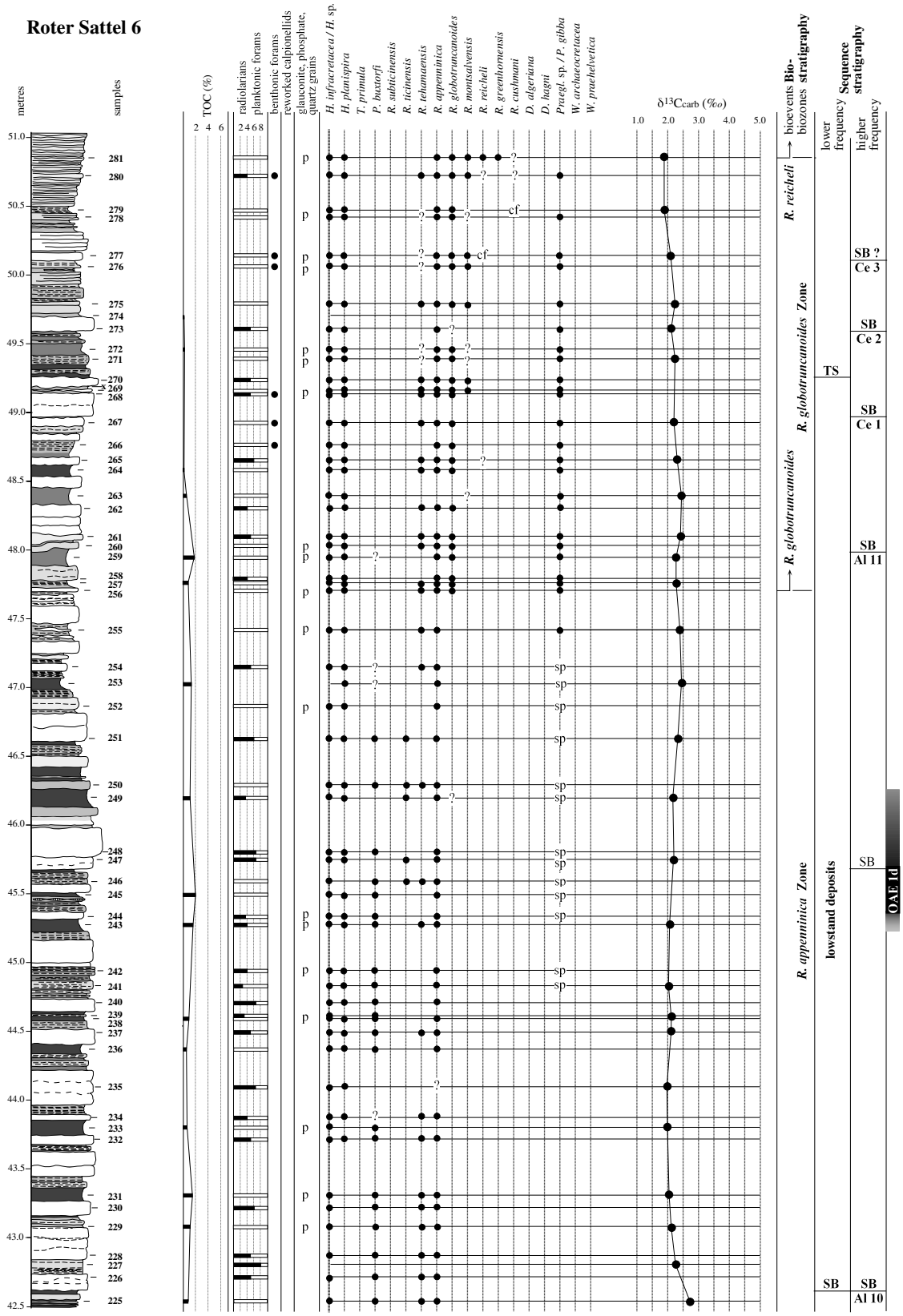
Roter Sattel 6
metres
samples
TOC (%)
radiolarians
planktonic forams
benthonic forams
reworked calpionellids
glauconite, phosphate, quartz grains
H. infracretacea / H. sp.
H. planispira
T. primula
P. buxtorfi
R. subticinensis
R. ticinensis
R. tehamaensis
R. apenninica
R. globotruncanoides
R. montsalvensis
R. reicheli
R. greenhornensis
R. cushmani
D. algeriana
D. hagni
Praegl. sp. / P. gibba
W. archaecretacea
W. praehelvetica
δ13Ccarb (‰)
bioevents
Bio-biozones
stratigraphy
Sequence stratigraphy
lower frequency
higher frequency
R. reicheli
R. globotruncanoides Zone
R. globotruncanoides
R. apenninica Zone
lowstand deposits
TS
SB
SB ?
Ce 3
Ce 2
Ce 1
Al 11
Al 10
OAE 1d

Figure 3 (f)

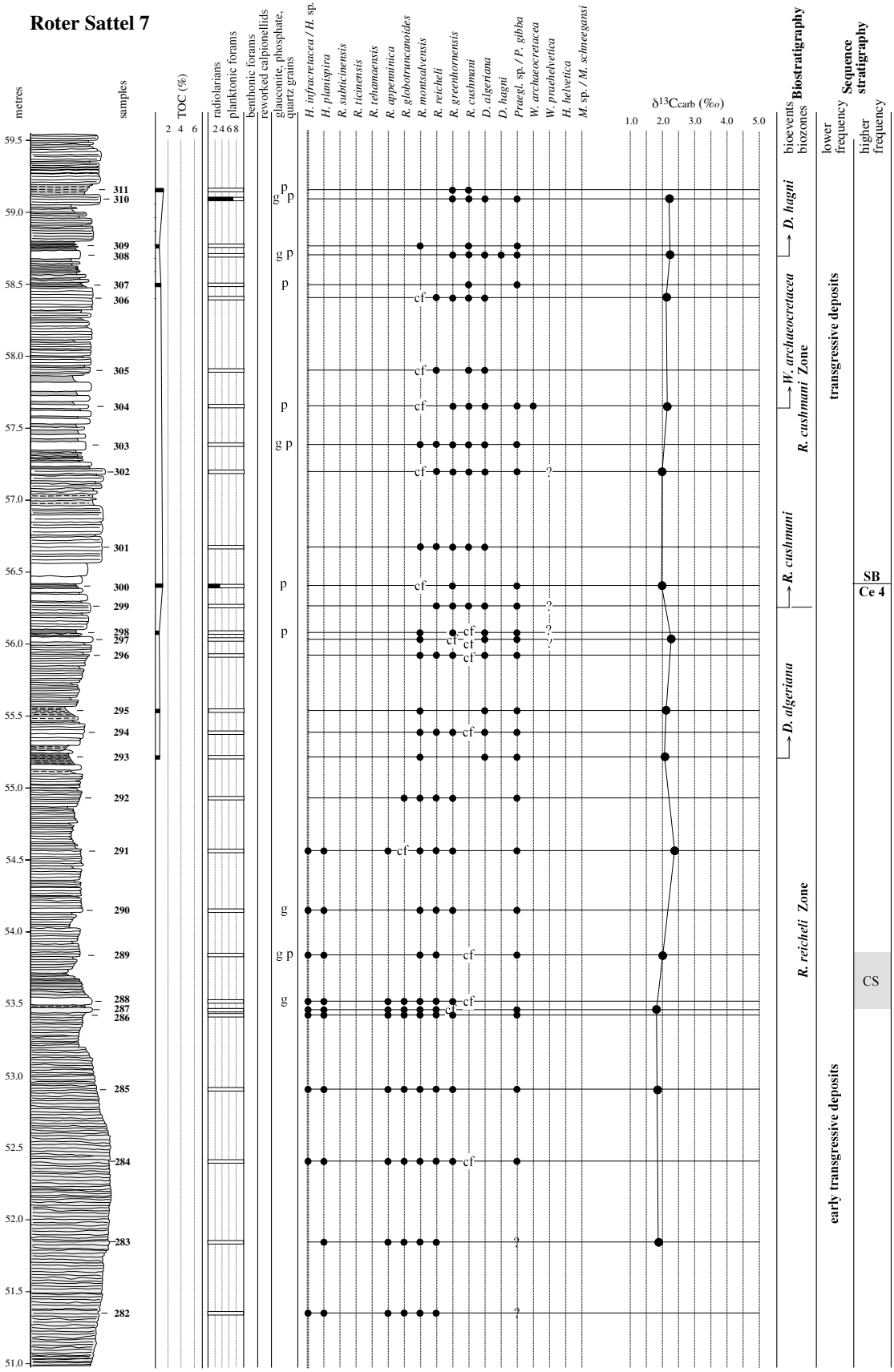
Roter Sattel 7
metres
samples
TOC (%)
radiolarians
planktonic forams
benthonic forams
reworked calpionellids
glauconite, phosphate, quartz grains
H. infracretacea / H. sp.
H. planispira
R. subticinensis
R. ticinensis
R. rehmaensis
R. appenninica
R. globotruncanoides
R. montsalvensis
R. reicheli
R. greenhornensis
R. cushmani
D. algeriana
D. hagni
Praegl. sp. / P. gibba
W. archaeocretacea
W. praehelvetica
H. helvetica
M. sp. / M. schneegansi
δ13Ccarb (‰)
bioevents
biozones
Biostratigraphy
D. hagni
W. archaeocretacea
R. cushmani Zone
R. cushmani
D. algeriana
R. reicheli Zone
lower frequency
transgressive deposits
early transgressive deposits
Sequence stratigraphy
higher frequency
SB
Ce 4
CS

Figure 3 (g)

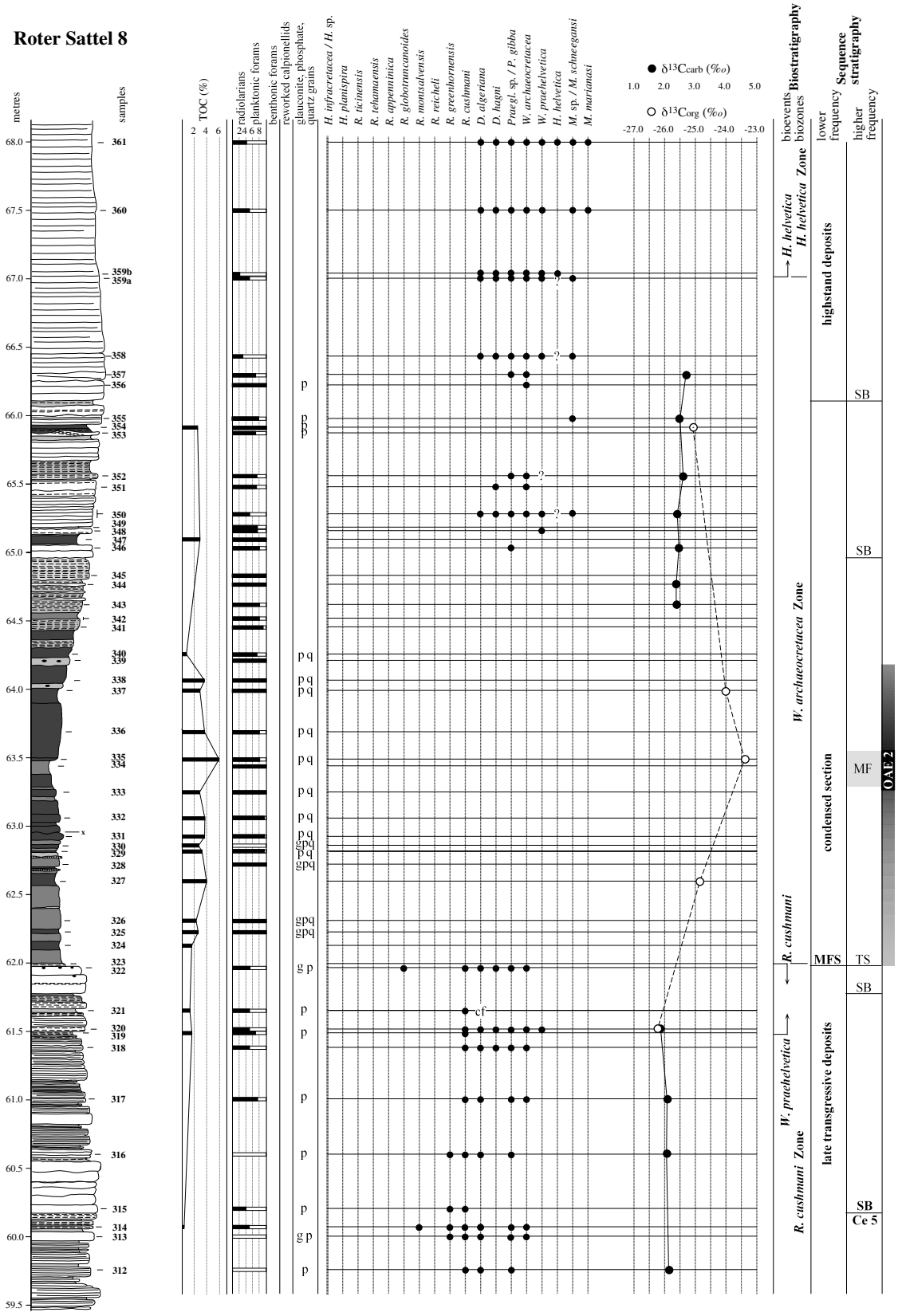
Roter Sattel 8
metres
samples
TOC (%)
radiolarians
planktonic forams
benthonic forams
reworked calpionellids
glauconite, phosphate, quartz grains
H. infracretacea / H. sp.
H. planispira
R. tieinensis
R. tehamaensis
R. appenninica
R. globotruncanoides
R. montsalvensis
R. reicheli
R. greenhornensis
R. cushmani
D. algeriana
D. hagni
Praegl. sp. / P. gibba
W. archaeocretacea
W. praehelvetica
H. helvetica
M. sp. / M. schmeegansi
M. marianasi
δ13Ccarb (‰)
δ13Corg (‰)
Biostratigraphy
bioevents
biozones
H. helvetica Zone
W. archaeocretacea Zone
R. cushmani
W. praehelvetica
R. cushmani Zone
Sequence stratigraphy
lower frequency
higher frequency
highstand deposits
condensed section
late transgressive deposits
SB
MF
MFS
TS
Ce 5
OAE 2

Figure 3 (h)

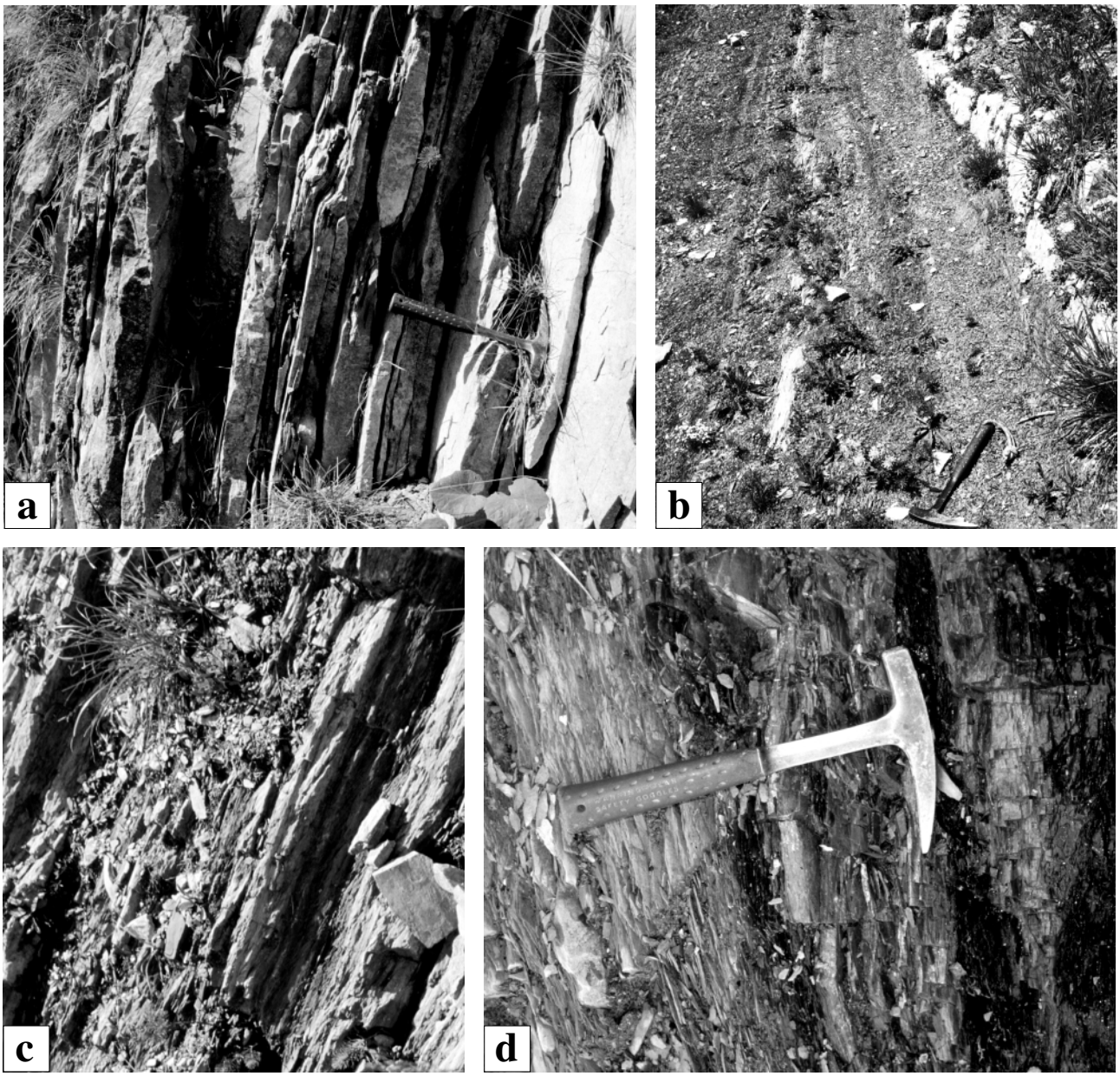

Figure 4. a, detail of limestone-dominated lithology, samples 312–316. b, detail of first black-shale interval, samples 21–30. c, detail of second black-shale interval, samples 175–200. d, detail of third black-shale interval, samples 336–341.

Carbonate migration during diagenesis has certainly enhanced the contrast between limestones and marls but has not masked the original pattern of varying carbonate-versus-clay ratio (Ricken & Eder, 1991). In marl-dominated intervals, the limestone beds are also generally marly.

3.2. *Marls*

Light to dark grey marls alternate with the limestone beds. The weathering profile in Figure 3 is more or less a reflection of the clay content, but no systematic calcimetric analyses have been performed, and exposure may have enhanced the degree of weathering locally. In common with the limestone beds, the marls are strongly bioturbated. Their faunal content is similar to that of the limestones, although enhanced carbonate dissolution may have destroyed part of the record. Pyrite can be abundant, and many marl layers contain iron concretions that may represent oxidized pyrite. Phosphate is more abundant than in the limestones and occurs as

particles or as impregnation of the matrix. Some marly intervals are silicified.

Owing to tectonic overburden, the clays show a relatively high crystallinity and cannot be used for environmental interpretation (J.-F. Deconinck, pers. comm., 1996). According to the palaeogeographic position of the section studied to the north of the Briançonnais High, however, it can be assumed that they have been washed in from there. Post-depositional compaction and carbonate dissolution enhanced the laminated texture of the marls by creating wavy clay seams. The microfossils, however, have not been compacted because of early diagenetic cementation.

3.3. *Black shales*

Some marls are black (Figure 3). They are concentrated in three intervals (Figure 4b–d) that define the three gullies at the outcrop (Figure 2). The faunal content is similar to that of the marls, with radiolarians and diatoms being particularly abundant (samples 22–39, 157–159, 331–354; Figure 3). Glauconite, phosphate, detrital quartz, and reworked calpionellids have their highest concentrations in the black shales. Authigenic quartz is common. Some samples contain abundant chlorophycean algae (*Botryococcus*; Figure 5g). Compositional changes created mm-scale laminations that were enhanced through compaction (Figure 5h).

Over the whole section, 102 samples have been analysed for total organic carbon (TOC; Gjermeni, 1999). Whereas TOC values generally are below 0.5% in limestones, they vary between 1 and 6.75% (max.) in the black marls. Hence, these deposits qualify as black shales (e.g., Jenkyns & Clayton, 1986; Weissert & Bréhéret, 1991). A total of 119 samples have been used for Rock-Eval analyses (Gjermeni, 1999). T_{max} values vary between 430 and 450°C and fall within the oil window (Espitalié *et al.*, 1985). The hydrogen index (mg HC/g TOC) is below 130 in the carbonate-dominated intervals but reaches 255, 360, and 395 in samples from the first, second, and third black-shale intervals, respectively.

The palynofacies of 43 samples have been examined (Gjermeni, 1999). Amorphous organic matter is predominant in the black-shale intervals (up to 80% in samples from the first and third intervals; 40% in the second interval), suggesting a contribution of marine organisms (Steffen & Gorin, 1993). Fluorescence is only weak because of oxidation and/or thermal maturation. Samples from the carbonate-rich units contain palynomacerals mainly of the PM4, PM4T, and PM1 groups, implying a more continental provenance of the organic material.

Dichloromethane-soluble organic matter has been extracted from ten black-shale samples (Gjermeni, 1999). Among the steranes, there is a predominance of C_{29} and lesser proportions of C_{28}, implying that much of this organic substance originated from (bacterially degraded) higher plants and a lesser proportion from marine zoo- and phytoplankton (Huang & Meinschein, 1979). The organic matter found in the Roter Sattel section thus appears to have a mixed marine and continental origin.

4. Biostratigraphy

The biozonation of the section studied has been established using planktonic foraminifera, which are generally abundant and well preserved (identification in thin section; marker species in Figures 6, 7). The definition of the biochronozones is based on Robaszynski & Caron (1995). Their *Ticinella praeticinensis* and *Rotalipora subticinensis* zones are, however, replaced by the *Biticinella breggiensis* Zone (*T. praeticinensis* and *R. subticinensis* becoming subzones; Bralower *et al.*, 1997). The distribution of the marker species, first and last occurrences in the section, and the biochronozones are indicated in the detailed log (Figure 3). In Figure 8, the zones are placed in the time-frame of Gradstein *et al.* (1995), according to Hardenbol *et al.* (1998).

The distribution through time of the marker species at Roter Sattel reflects the classical succession of foraminiferal events (Premoli Silva & Sliter, 1994; Robaszynski & Caron, 1995). Most limits between the biozones are well defined; some, however, are transitional or uncertain. Abrupt biozone boundaries occur in the Upper Albian–Upper Cenomanian interval (samples 198–322; Figure 3e–h): the planktonic foraminifera are abundant and diversified, especially the species with complex tests (*Rotalipora*). This group shows a rapid evolution, implying good adaptation to a stable, oxygenated and oligotrophic environment. The record of this evolution is well preserved, and there was no major reworking or dissolution of tests. An abrupt biozone boundary also occurs between samples 322 and 323 (Figure 3h). The sudden change from light-coloured limestones with nannofossils and well-diversified planktonic foraminifera to black shales dominated by radiolarians suggests rapid eutrophication of the surface waters, or progressive eutrophication but sedimentary condensation (see section 5.6 below). Planktonic productivity dropped, and acid bottom waters precluded the preservation of most carbonate tests.

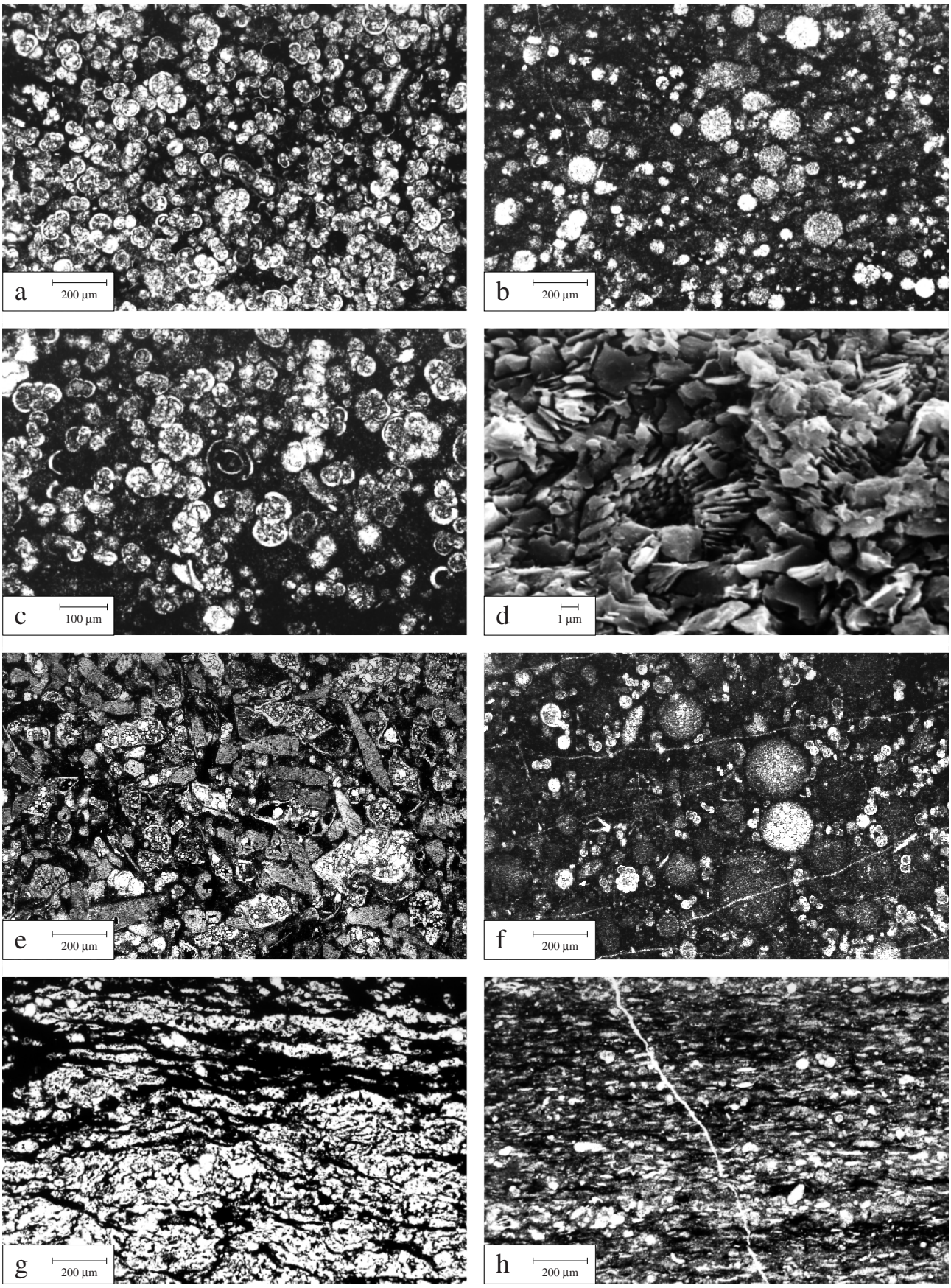
a
200 µm
b
200 µm
c
100 µm
d
1 µm
e
200 µm
f
200 µm
g
200 µm
h
200 µm

A transition between two biozones (*Whiteinella archaeocretacea–Helvetoglobotruncana helvetica*) is indicated by the interval between samples 346–358 (Figure 3h). The siliceous black marls with radiolarians and diatoms still indicate eutrophic conditions for samples 347, 352, and 354. Comparable concentrations of diatoms have been recognized in other black shales at the Cenomanian/Turonian boundary. In the Agadir section in Morocco, diatoms accompany (and locally precede) radiolarian blooms in the *W. archaeocretacea* Zone (Terrab, 1996). They are interpreted as indicators of nutrient input related to upwelling. The limestone beds (samples 350, 355, and 358) already contain a relatively diversified association of planktonic foraminifera. However, the marker species *H. helvetica* is not yet present. This can be explained by the fact that its life cycle probably needed well-oxygenated conditions in deep water (Caron, 1983). *H. helvetica* appeared only when fully oligotrophic and oxic conditions throughout the water column were restored (sample 359; Figure 3h). *H. helvetica* evolved from *Whiteinella praehelvetica* by developing one keel on the last whorl. This step is used as a global biostratigraphical marker (Robaszynski & Caron, 1995). However, on a regional scale, the first appearances of *H. helvetica* are variable. At Pueblo (USA), this foraminifer appears at the base of the *Watinoceras devonense* ammonite Zone that indicates the base of the Turonian (Morel, 1998). At Oued Smara (Tunisia), where the Cenomanian/Turonian boundary is marked by an important anoxic event, *H. helvetica* is recorded only in the middle Turonian *Kamerunoceras turonense* ammonite Zone (equivalent to the *Collignoniceras woollgari* Zone; Robaszynski *et al.*, 1990). At Roter Sattel, rare specimens of *H. helvetica* are found for the first time 2.5 m above the black-shale interval (in sample 359), whereas a well-diversified association of double-keeled planktonic foraminifera is present already in the limestone beds of sample 350 (Figure 3h). This diachronism thus depended on local palaeogeographic conditions that modulated the impact of the oceanic anoxic event.

The boundary between the *Leupoldina cabri* and *Globigerinelloides ferreolensis* zones (samples 105–128; Figure 3c) is uncertain because the occurrences of *L. cabri* and *G. ferreolensis* are doubtful. This may be the result of dilution by a high sedimentation rate around sequence boundary Ap 4 (see section 5.4 below). Although globally defined as a total range zone (Robaszynski & Caron, 1995), the *L. cabri* Zone at Roter Sattel has an uncertain upper limit.

5. Sequence-stratigraphic and environmental interpretation

Based on facies evolution and stacking pattern of beds and bed-sets, the Roter Sattel section is interpreted in terms of sequence stratigraphy (e.g., Vail *et al.*, 1991). In one section alone, the large-scale geometries of the sedimentary bodies cannot be seen, and we therefore speak of lowstand, transgressive, and highstand deposits (according to the evolution of facies and stacking pattern) instead of systems tracts. Comparison with sequences that are well established in European basins (Hardenbol *et al.*, 1998) then enables us to distinguish between sequences created by regionally or globally recognized eustatic sea-level changes and sequences resulting from tectonic activity or local sedimentary processes. For the correlatable sequence boundaries (SB) we use the labels of Hardenbol *et al.* (1998). The sequences are indicated in Figures 3 and 8.

5.1. Criteria used for sequential interpretation

Several types of sedimentation style are observed, defined by characteristic stacking patterns, limestone-marl ratios, and facies. For each type, a sedimentological and sequence-stratigraphic explanation can be proposed.

Intervals dominated by relatively thick limestone beds and only reduced marly layers suggest that nannoplankton productivity was high and clay input reduced. This combination could have occurred when sea level was below the platform edge, thus cutting out clay transport across the platform to the ocean and concentrating planktonic productivity above the slope (Scholle *et al.*, 1983; Vail *et al.*, 1991; Strohmenger & Strasser, 1993; Milliman & Droxler, 1996). Nutrients

Figure 5. a, photomicrograph of planktonic foraminifer-rich packstone, sample 151, *T. bejaouaensis* Zone. b, radiolarian-rich siliceous packstone, sample 140, *G. algerianus* Zone. c, reworked calpionellids in wackestone-packstone, sample 149b, *G. algerianus* Zone. d, SEM photograph of nannoconid limestone, sample 12, *G. blowi* Zone. e, photomicrograph of grainstone composed of planktonic foraminifera and inoceramid prisms, sample 284, *R. reicheli* Zone. f, packstone rich in radiolarians and planktonic foraminifera, sample 209, *R. ticinensis* Zone. g, compacted *Botryococcus* colonies in organic-rich matrix, sample 173, *H. planispira* Zone. h, radiolarians, diatoms, small benthic foraminifera, and quartz grains forming laminae in second black-shale interval, sample 158, *H. planispira* Zone.

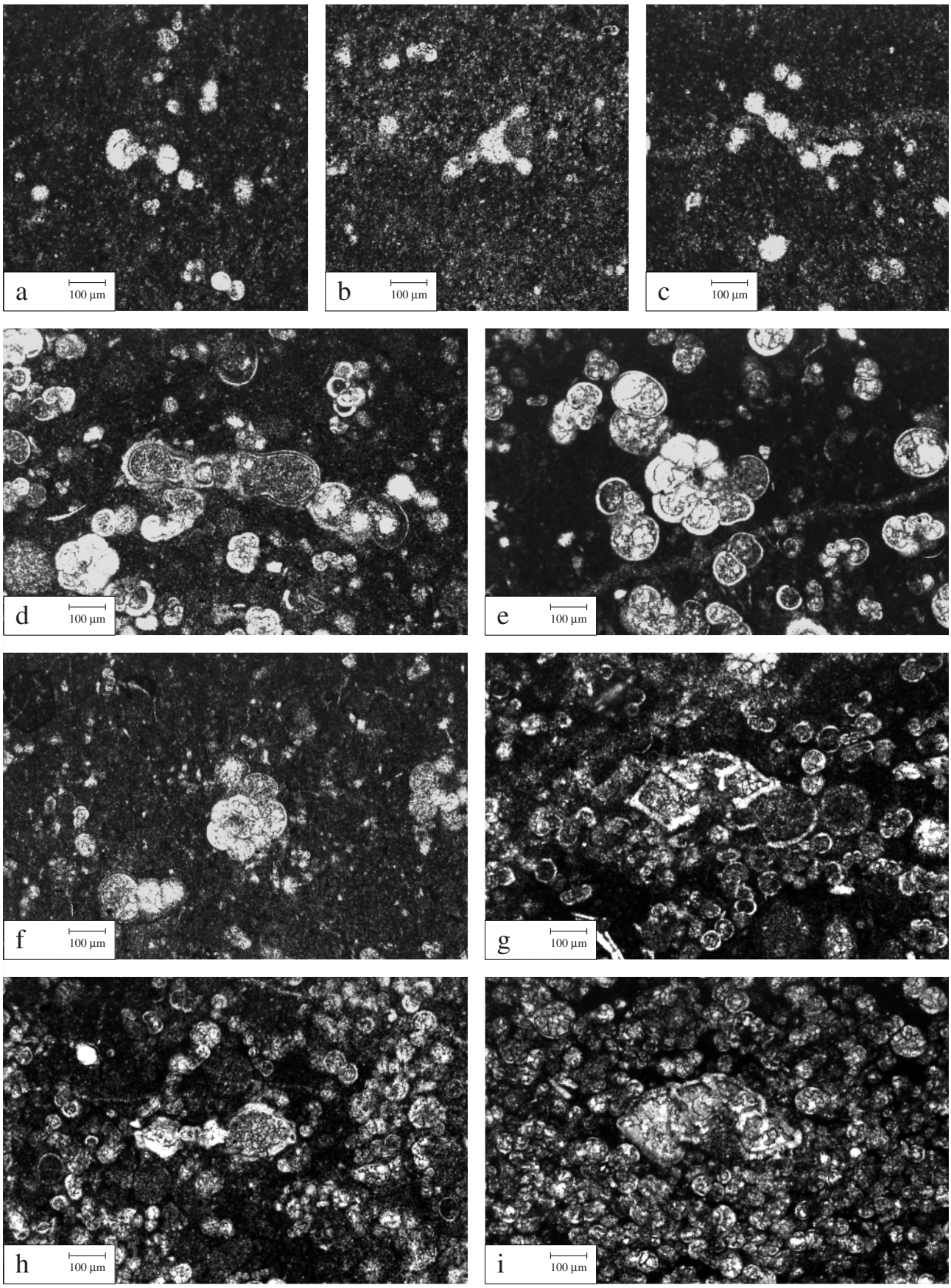
a
100 µm
b
100 µm
c
100 µm
d
100 µm
e
100 µm
f
100 µm
g
100 µm
h
100 µm
i
100 µm

for blooms of planktonic organisms were furnished by upwelling currents and more vigorous oceanic circulation (Erba *et al.*, 1992). Benthic material and reworked particles are common. Laterally changing bed thicknesses and irregular bedding planes indicate channeling. Such intervals are therefore interpreted as lowstand deposits (possibly belonging to a slope fan).

Relatively thick limestone beds and thick marly layers suggest that sea level was still low but episodically allowed clays to be transported across the platform. The corresponding interval is interpreted as a lowstand, possibly indicating a lowstand wedge (some of these intervals display a thickening-upward trend in the limestone beds, implying a relative shallowing upward).

Intervals dominated by marls or marly limestones and generally displaying only thin limestone beds are interpreted as transgressive deposits. The platform being flooded, carbonate productivity was distributed over a larger area and, consequently, was less concentrated above the slope (Scholle *et al.*, 1983). The ocean reached the source areas of siliciclastics, and clays were easily transported across the platform into the basin. Reworking still occurred, but the particles were smaller than in lowstand deposits. An increase in land-derived nutrients led to blooms of radiolarians (De Wever *et al.*, 1994; Erbacher & Thurow, 1997). Enrichment of the sediment in organic matter was owing to dysoxic or anoxic conditions of bottom waters, suggesting increased nutrient cycling and expansion of the oxygen-minimum zone (Weissert & Mohr, 1996; Erbacher & Thurow, 1997). Black shales commonly formed in transgressive intervals (Schlanger & Jenkyns, 1976).

Marly intervals that are strongly enriched in organic matter correspond to maximum flooding and condensation (e.g., Loutit *et al.*, 1988). Pelagic and hemipelagic carbonate production was at its minimum. Oceanic circulation slowed down. Bottom waters were oxygen-deficient and more acid, which led to preservation of organic matter but dissolution of carbonate particles. Planktonic-foraminifer marker species can, therefore, be difficult to find in these intervals. The black marls may contain phosphate and silica, implying reduced sedimentation rates.

Carbonate-dominated intervals with relatively thin limestone beds evolving from a marly interval are interpreted as highstand deposits. In some cases there is a thickening-upward trend in the limestone beds. This is the expression of a slow down in relative sea-level rise, forcing nannoplankton production basinwards. Part of the muddy carbonate fraction may also have been derived from the platform (e.g., Milliman *et al.*, 1993).

Sequence boundaries are placed at the base of the thickest limestone beds, or at the base of a carbonate-dominated interval where a break in stacking pattern occurs.

In Figure 3, two orders of sequences have been distinguished: long-term, million-year-scale sequences comparable to the tectono-eustatic second-order sequences of Vail *et al.* (1991), and short-term sequences related to higher-frequency changes of sea level and/or climate. The latter have been indicated where sedimentological criteria permit and have no *a priori* time significance. However, it is likely that several of these higher-frequency changes are linked to the 400-ka orbital cycle of eccentricity (Strasser *et al.*, 1999; see also section 6.2).

5.2. *Limestone-marl alternations*

Limestone-marl alternations are common in hemipelagic and pelagic settings, and it can be shown that many of them are related to climatic cycles in the Milankovitch frequency band (examples and discussion in Einsele & Ricken, 1991). Climatic changes affected sea level and rainfall in the hinterland, thus influencing clay input and at the same time oceanic circulation, nutrient cycling, and water temperature that controlled planktonic productivity (Erba *et al.*, 1992; Mattioli, 1997). High-frequency fluctuations of the carbonate compensation depth as a controlling factor of the limestone-marl alternations at Roter Sattel can be excluded because the marls contain calcareous fossils.

The limestone-marl alternations that constitute a large part of the section studied commonly group into bundles (Figure 3). However, a hierarchy of bundling reflecting the Milankovitch parameters (Berger *et al.*, 1989) can be recognized only in certain intervals. For example, at the very base of the section (samples 2–15; Figure 3a), 21 limestone beds group into four sets of 4–6 beds each. This bundling may correspond to the 400-ka orbital eccentricity cycle, with one

Figure 6. Photomicrographs of planktonic-foraminifer marker species. a, *Globigerinelloides blowi*, sample 42. b, *Leupoldina cabri*, sample 42. c, *Leupoldina cabri*, sample 64. d, *Globigerinelloides algerianus*, sample 149c. e, *Ticinella bejaouaensis*, sample 151b. f, *Ticinella primula*, sample 191. g, *Rotalipora subticinensis*, sample 202. h, *Planomalina buxtorfi*, sample 209. i, *Rotalipora ticinensis*, sample 199.

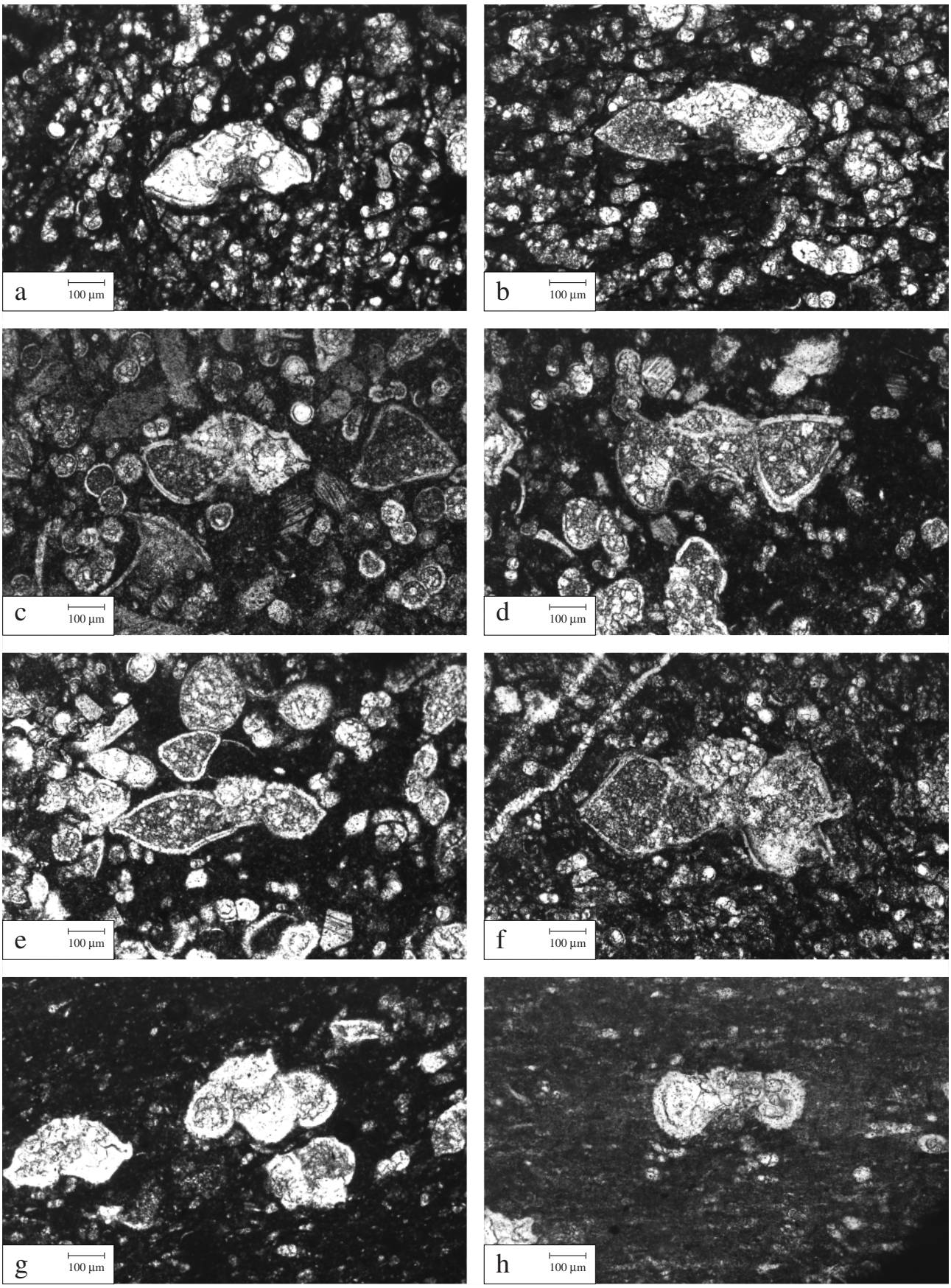
a
100 µm
b
100 µm
c
100 µm
d
100 µm
e
100 µm
f
100 µm
g
100 µm
h
100 µm

limestone bed or limestone-marl couplet corresponding to the 20-ka precession cycle, and a bedset to the 100-ka eccentricity cycle. Because of condensation in the black-shale intervals and potential erosion within the lowstand deposits it is unfortunately not possible to establish a cyclostratigraphy for the interval studied, and the duration of a limestone-marl couplet can only be speculated upon. Furthermore, it is quite possible that the mechanisms responsible for the formation of these couplets changed through time.

The different types of stacking pattern of limestone-marl alternations and the varying limestone-clay ratios that have been used to define the large-scale sequence-stratigraphic units can be explained by the superposition of high-frequency (possibly orbitally controlled) sea-level and climatic fluctuations on a long-term (million-year scale) trend of sea level and climate change. Owing to this superposition, diagnostic sequence-stratigraphic surfaces may be multiplied (Pasquier & Strasser, 1997). In Figure 3, the most obvious surfaces have been chosen, but they may be offset by one or two beds or bed-sets when compared to other sections.

5.3. *Base of section to top of first black-shale interval*

The base of the section is composed of a thick package of locally channelized limestone beds interpreted as lowstand (slope fan) deposits (Figure 3a). The thickening-upward trend of the following limestone package may be attributed to a lowstand wedge, and a well-developed transgressive surface (below sample 22) leads into the first black-shale interval.

High-resolution correlation with the Cismon section in Italy (Erba *et al.*, 1999) indicates that the magnetic polarity chron M0r ends just below the higher-frequency sequence boundary at 1.8 m at Roter Sattel (Hochuli & Strasser, 2000). This suggests that the lowermost sequence boundary recognized in the section most probably corresponds to sequence boundary Ap 2 of Hardenbol *et al.* (1998), which is situated within both M0r and the *Globigerinelloides blowi* Zone.

The top of the thick limestone beds (sample 21) corresponds to the nannoconid crisis of Erba (1994) and Erba *et al.* (1999), which precedes OAE 1a. In the Roter Sattel section, TOC-rich marls occur in the upper part of the *G. blowi* Zone, thus correlating well with the globally recognized anoxic event (e.g., Jenkyns 1980; Larson *et al.* 1993; Erba *et al.*, 1999). The carbon isotopes show the characteristic positive shift recognized in many other sections (e.g., Selli Level; Menegatti *et al.*, 1998). In silicified samples of the well-studied section of Cismon (Italy), the foraminifer *L. cabri* is present already at the base of OAE 1a but becomes abundant only above the anoxic event (Erba *et al.*, 1999; Premoli Silva *et al.*, 1999). At Roter Sattel, the first *L. cabri* has been found in the overlying carbonate-rich interval (sample 42; Figure 3a).

Channelled limestone beds (sample 26) and a thinly-bedded limestone package (sample 28) are interpreted as lowstand deposits of a higher-frequency sequence that punctuate the generally transgressive to maximum-flooding conditions of the black shales. The corresponding sequence boundary is interpreted as being the equivalent of Ap 3, which just post-dates the nannoconid crisis (Hardenbol *et al.*, 1998). Also the limestone bed of sample 34 is interpreted as a small-scale lowstand. These two higher-frequency sequences display well-developed condensed sections or maximum-flooding intervals because they formed during a lower-frequency transgressive to maximum-flooding trend of sea-level evolution. It is noteworthy that reworked calpionellids are concentrated within the black-shale interval (samples 27–40). Although long-term sea level was rising, erosion of Upper Jurassic–lowermost Cretaceous material must have occurred, most probably in canyons on the slope or on tectonically created escarpments.

5.4. *Top of first to base of second black shale*

With the limestone bed of sample 40 (Figure 3a), the lithology becomes carbonate-dominated again. Thick and locally channelized beds alternate with more marl-dominated intervals. These alternations are interpreted as resulting from higher-frequency cycles, but it is difficult to consider the irregular stacking in terms of orbital cyclicity. The general trend, however, shows an upward enrichment in carbonate. An important sequence boundary is placed at the base of thick and channelled limestone beds (samples 118–124, Figure 3c). It is situated within the uncertainty interval between the *L. cabri* and *G. ferreolensis* zones

Figure 7. Photomicrographs of planktonic-foraminifer marker species. a, *Rotalipora tehamaensis*, sample 217. b, *Rotalipora appenninica*, sample 217. c, *Rotalipora globotruncanoides*, sample MC 560/2, equivalent 285. d, *Rotalipora reicheli*, sample MC 559/1, equivalent 290/291. e, *Rotalipora montsalvensis*, sample MC 559/1, equivalent 290/291. f, *Rotalipora cushmani*, sample MC 988/2, equivalent 320. g, *Whiteinella archaeocretacea*, sample 358. h, *Whiteinella praehelvetica*, sample 359.

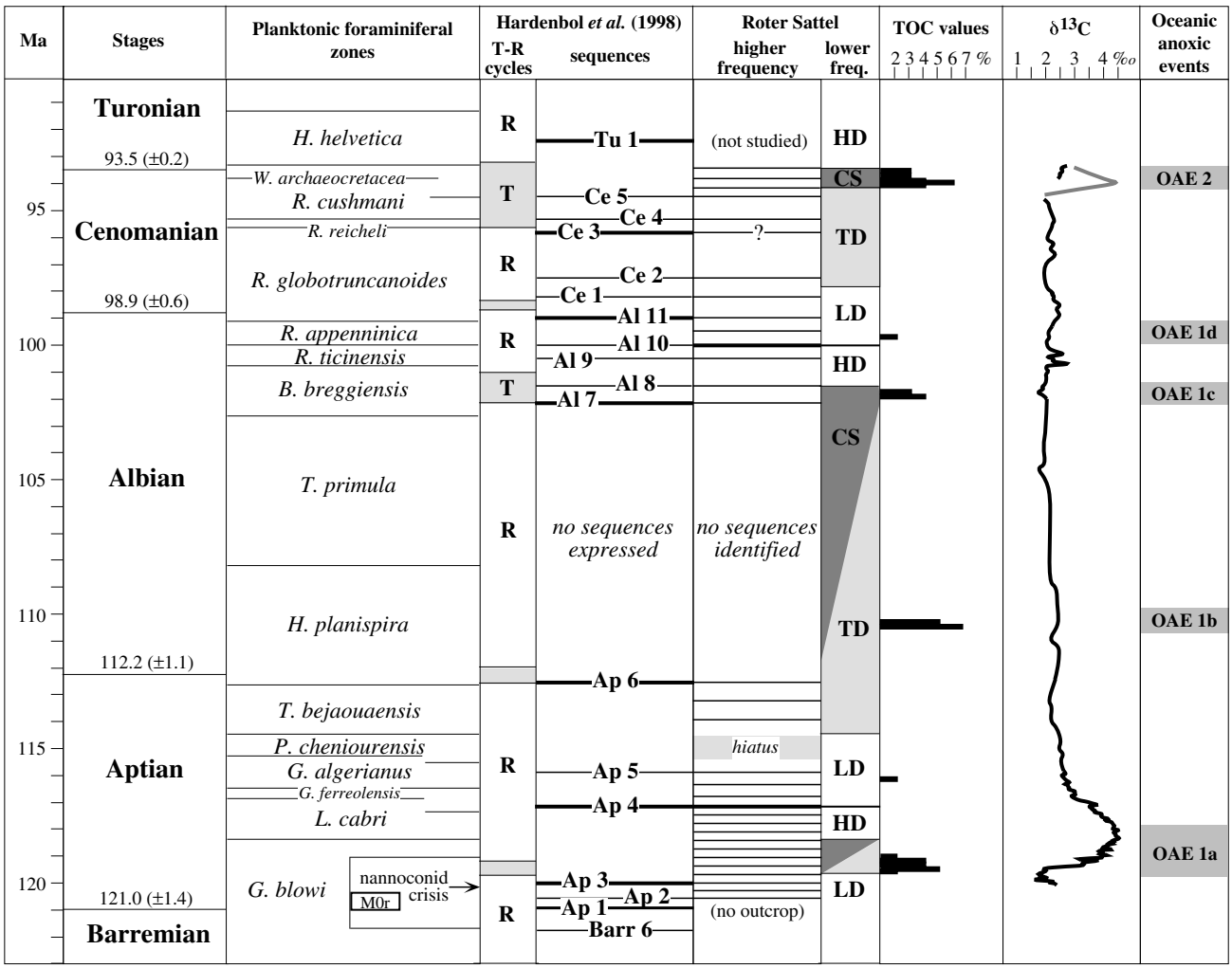

Figure 8. Synoptic chart of biochronozones (Robaszynski & Caron, 1995; Bralower *et al.* 1997), sequence boundaries of Hardenbol *et al.* (1998), and sequence boundaries identified in the Roter Sattel section. The absolute time scale is according to Gradstein *et al.* (1995). The total organic carbon (TOC) has been indicated only for values of >1%; the position of the peaks is estimated according to the sequence-stratigraphic position of the samples analyzed. Carbon-isotope curve simplified after Menegatti *et al.* (1998) and Gjermeni (1999); oceanic anoxic events (OAEs) according to Jenkyns (1980), Larson *et al.* (1993), Bralower *et al.* (1994), and Erbacher & Thurow (1997). LD, lowstand deposits; TD, transgressive deposits; CS, condensed section and/or maximum flooding; HD, highstand deposits. For discussion, see text.

and thus corresponds to sequence boundary Ap 4 of Hardenbol *et al.* (1998) (Figure 8).

The irregular alternations of thick limestone beds and thick marly intervals from sample 118 up to 150 (Figure 3c, d) suggest lowstand conditions in the lower-frequency sequential evolution. The thick limestone packages are interpreted as lowstand deposits of higher-frequency sequences, whereas the more marly and thinner-bedded intervals generally represent transgressive and highstand deposits of these sequences. The sequence boundary at the top of the *G. algerianus* Zone most probably corresponds to Ap 5 of Hardenbol *et al.* (1998). Samples 137 and 142 have relatively elevated TOC values when compared to the rest of this interval (Figure 3d). This may be regarded as heralding the following black-shale interval and results from a superposition of higher-frequency cycles on the beginning transgressive trend of the lower-frequency evolution.

Sample 149e, which is very rich in planktonic foraminifera, contains the last *G. algerianus* and thus indicates the top of this zone (Figure 3d). *Ticinella bejaouaensis* appears in sample 150a. *Planomalina cheniourensis* is already present in sample 149a, but the base of the corresponding zone is defined by the last appearance of *G. algerianus* and its top by the first

appearance of *T. bejaouaensis* (Robaszynski & Caron, 1995). Hence, according to this definition, the *P. cheniourensis* Zone is not represented at Roter Sattel, although it encompasses about 700 ka (Hardenbol *et al.*, 1998). This may be explained by reworking and erosion in the top of the lowstand deposits of sequence Ap 5, and a hiatus must be postulated somewhere between samples 149e and 150a.

5.5. *Second black-shale interval*

Dominated by dark grey to black marls, this interval (samples 151–195; Figure 3d, e) is interpreted as a lower-frequency transgressive deposit. Several limestone beds punctuate it and may suggest sea-level fluctuations, but stratigraphic sequences are difficult to define. This is consistent with the chart of Hardenbol *et al.* (1998). High TOC values in the *Hedbergella planispira* Zone relate to OAE 1b, and a second peak in TOC in the *B. breggiensis* Zone to OAE 1c (Figure 8). However, there is no change in the carbon-isotope values associated with these black shales.

The base of the channelled and siliceous limestone beds (sample 164) is interpreted as a high-frequency sequence boundary corresponding to Ap 6, and the base of the limestone package (samples 185–188) as corresponding to sequence boundary Al 7 of Hardenbol *et al.* (1998) (Figure 8).

Reworked calpionellids indicate erosion of pre-existing sediment. Detrital quartz points to increased terrigenous run-off, a more proximal position, and/or different source material when compared to the first black-shale interval. Benthic foraminifera may indicate somewhat shallower environments. Sample 173 is rich in silicified *Botryococcus* (Figure 5g), suggesting input from very shallow, freshwater or brackish environments. Consequently, this TOC-rich interval (Figure 3e) is not interpreted as a condensed section but rather as corresponding to the maximum flooding when shallow platform areas were inundated and material from there was mobilized.

5.6. *Succession between second and third black shale*

The first part of this succession (samples 196–225) is interpreted as a highstand on the lower-frequency trend (Figure 3e). From samples 226 to 270, thick limestone beds alternate with thick and locally black marl layers (Figure 3f), which are regarded as lower-frequency lowstand deposits. Higher-frequency sequence boundaries have been placed at the bases of the thickest limestone beds. According to their biostratigraphic position, they may correspond to sequence boundaries Al 9, Al 10, Al 11, and Ce 1 of Hardenbol *et al.* (1998), of which Al 10 is considered to be the most important, separating a lower-frequency highstand from a lowstand.

The relatively high TOC values in the *Rotalipora appenninica* Zone (sample 245) correlate well with OAE 1d (Figure 8). However, no carbon-isotope shift is associated, and the elevated TOC occurs in a lower-frequency lowstand. A lower-frequency transgressive surface has been placed at the top of bed 270. The carbonate beds containing samples 273 and 277 are interpreted as smaller-scale lowstand deposits, possibly associated with sequence boundaries Ce 2 and Ce 3 of Hardenbol *et al.* (1998).

An important change of facies and stacking pattern occurs at the level of sample 279; the sediment becomes reddish, coarser-grained, dominated by planktonic foraminifera, and enriched in inoceramid prisms. The grainstone texture (Figure 5e) and the wavy sedimentary structures indicate strong bottom currents. This type of sediment more or less encompasses the *Rotalipora reicheli* Zone (Figure 3g), suggesting that 5.5 m (compacted) of sediment accumulated within about 200 ka. Such high accumulation rates are possible on contourite drifts (Stow, 1994). The thicker limestone beds of samples 287 and 288 may indicate condensation: a colour change from reddish to grey occurs just below, and glauconite and phosphate grains are concentrated above (Figure 3g).

The following higher-frequency sequence boundary has been placed at the base of thicker limestone beds (above sample 300). It coincides with the base of the *Rotalipora cushmani* Zone and thus correlates with Ce 4 of Hardenbol *et al.* (1998). Grainstones are abundant up to sample 316 and indicate winnowing by bottom currents or storm waves (Python-Dupasquier, 1990).

The package of thicker limestone beds including sample 315 implies a lowstand, with a sequence boundary equivalent to Ce 5 (Figure 3h). The following higher-frequency sequence boundary is implied by the carbonate beds containing sample 322 but has no correspondence on the chart of Hardenbol *et al.* (1998). The iron-stained surface of this limestone package may be interpreted as having formed during a second transgressive pulse on the lower-frequency sea-level trend, or as a lower-frequency maximum-flooding surface (enhanced by a higher-frequency transgressive surface) at the base of the condensed section.

5.7. *Third black-shale level and top of section*

With sample 323, the third black-shale episode starts. As in the previous black-shale intervals, radiolarians

and detrital quartz are relatively abundant. The high TOC contents and the positive shift of carbon isotopes (measured on organic matter because of a lack of carbonate; Gjermeni, 1999) tie in well with OAE 2 (Figure 8). The interval is interpreted as consisting of deposits related to maximum flooding and condensation, especially at the level of sample 334 with the highest TOC value, situated in the *W. archaeocretacea* Zone. This is in contrast to the chart of Hardenbol *et al.* (1998) where the condensed section of the corresponding T-R cycle is placed at the base of the *H. helvetica* Zone (Figure 8). From sample 346 upwards, increasing carbonate content heralds lower-frequency highstand conditions, but the base of this highstand has been placed where the marly layers disappear. Two higher-frequency sequence boundaries are identified at the bases of relatively massive carbonate beds.

6. Discussion

Based on the above interpretation of facies and depositional sequences, the Roter Sattel section can now be placed in both a regional and a global context. Comparison with time-equivalent sections makes it possible to filter out local tectonic and sedimentological events and evolutions, and to define how the Subbriançonnais Domain was influenced by regional and global oceanographic changes.

6.1. Local, regional, and global record

Some 6 km to the NNE of Roter Sattel, Gjermeni (1999) logged the section of Chällihorn, covering the same time-span as that at Roter Sattel. The three black-shale intervals as well as the higher-frequency sequences are easy to correlate between the two sections. However, a bed-to-bed correlation is possible only in a few selected intervals, implying that gravitational processes and/or bottom currents partly redistributed the sediment, and that the environmental thresholds that led to the limestone-marl alternations may have varied from one location to another. Thicknesses of the higher-frequency sequences differ by up to 50%, but the thicknesses between the transgressive surface at base of the first black shale and that at the base of the third black shale differ by only 4 m (59 m at Roter Sattel vs. 55 m at Chällihorn). This testifies to relatively stable tectonic conditions on a local scale. At the scale of the Romandes Prealps, however, important thickness and facies variations of the Intyamon Formation and hiatuses imply tectonic activity. These led Python-Dupasquier (1990) to define four ENE–WSW striking basin compartments created by differential subsidence.

In the Chablais Prealps, some 50 km to the WSW (Figure 1), Hable (1997) has presented a detailed and biostratigraphically well-constrained analysis of the Aptian–Turonian interval. Intense synsedimentary block-faulting created many hiatuses and extreme variations in sediment thicknesses. Where preserved, dark lithologies rich in organic matter occur in the *H. planispira* and *T. primula* zones (OAE 1b?) and in the *R. cushmani* Zone (OAE 2?), but also in other positions which have no global equivalent. Some, but not all, sequence boundaries of Hardenbol *et al.* (1998) were recognized. Consequently, it was concluded that tectonic activity in the palaeogeographic domain of the Chablais Prealps created basins and highs that behaved independently, and that global signals were partly obliterated or distorted.

In Chablais, the top of the *G. algerianus* Zone is commonly marked by a hardground, and sediments of the *P. cheniourensis* and *T. bejaouaensis* zones are missing (Hable, 1997). At Roter Sattel, only the *P. cheniourensis* Zone is missing (see section 5.4), but elsewhere in the Romandes Prealps, the *H. planispira* and *T. primula* zones are also missing or condensed (Python-Dupasquier, 1990). In Cismon (Italy), the *G. algerianus*, *P. cheniourensis*, *T. bejaouaensis*, and *H. planispira* zones are not recorded (Erba *et al.*, 1999). It thus appears that around the Aptian/Albian boundary, non-deposition, condensation, and/or tectonic uplift causing erosion occurred on a regional scale. The beginning of tectonic inversion that eventually led to the Alpine orogeny is documented in the Prealps from the same time interval (Dall'Agnolo, 2000).

The fact that the section at Roter Sattel has recorded all globally recognized oceanic anoxic events (Jenkyns, 1980; Bralower *et al.*, 1994; Larson *et al.*, 1993; Erbacher & Thurow, 1997), as well as most of the sequence boundaries identified in European basins by Hardenbol *et al.* (1998), suggests that sedimentation there took place in a relatively stable, slowly subsiding basin compartment. Sedimentation rates varied considerably through time, but facies and stacking patterns imply that this was caused mainly by varying sediment supply rather than by dramatic changes in subsidence.

6.2. Eustasy, oceanic circulation, and climate changes

The massive limestone beds at the base of the section represent the end of a lower-frequency regressive trend of sea-level evolution identified by Hardenbol *et al.* (1998) in many European basins, as well as by Haq *et al.* (1987) on a global scale. From then onwards, there is a general sea-level rise up to its highest Phanerozoic stand in the *W. archaeocretacea*

Zone (Haq *et al.*, 1987). Superimposed on this long-term trend are fluctuations that were probably driven by tectono-eustasy, termed lower-frequency in Figures 3 and 8. These were again modulated by higher-frequency sea-level changes. Many of the higher-frequency sequences identified at Roter Sattel have estimated durations of one or several 100 ka and could possibly correspond to fluctuations driven by the first and second eccentricity cycle of the Earth's orbit (100 and 400 ka; Berger *et al.*, 1989). Where such cycles are enhanced by a longer-term eustatic trend and/or a change in subsidence pattern, sequence boundaries in the sense of Hardenbol *et al.* (1998) are recorded (Figure 8; see also Strasser *et al.*, 1999). The discrepancies between the transgressive-regressive facies cycles (T-R cycles in Figure 8) of Hardenbol *et al.* (1998) and our interpretation of the deposits composing the lower-frequency sequences at Roter Sattel may be explained by local variations in the ratio of sea-level change vs. sediment supply (e.g., Pasquier & Strasser, 1997), and by shifting of diagnostic surfaces because of superposition of higher-frequency cycles (e.g., Strasser *et al.*, 1999).

The long-term sea-level rise was most probably related to the emplacement of the Ontong-Java Plateau basalts during the early Aptian (e.g., Larson, 1991). This was accompanied by an elevation of pCO_2, greenhouse conditions, accelerated water cycle, increased nutrient input into the ocean, increased organic productivity and burial of organic matter, black-shale formation, and environmental changes affecting planktonic organisms (e.g., Tarduno *et al.*, 1991; Larson & Erba, 1999; Gröcke *et al.*, 1999). The positive shift of $\delta^{13}C$ at about 120 Ma may correspond to the maximum of volcanic activity (Larson & Erba, 1999). At Roter Sattel, these processes are recorded in the first black-shale interval. Hence, this interval is the equivalent of OAE 1a, represented also by, e.g., the Selli Level in Italy (e.g., Coccioni *et al.*, 1992; Larson *et al.*, 1993; Baudin *et al.*, 1998; Erba *et al.*, 1999), the Goguel level in the Vocontian Trough in France (e.g., Bréhéret, 1988; Weissert & Bréhéret, 1991), and by an organic-rich layer on Pacific guyots associated with a positive $\delta^{13}C$-shift (Jenkyns, 1995; Röhl & Ogg, 1996).

Detrital quartz, a high proportion of terrestrially derived organic matter, and relative abundance of radiolarians implying nutrient input suggest that the transgression reached terrigenous source areas (Erbacher & Thurow, 1997) or remobilized terrigenous material stored on the shallow platform (Dunbar *et al.*, 2000). Platform drowning that was time-equivalent to the OAE 1a has been documented in several areas: e.g., the Urgonian Platform in France and Switzerland (Hunt & Tucker, 1993; Föllmi *et al.*, 1994), the Abruzzi Platform in Italy (D'Argenio *et al.*, 1993), and the isolated Mount Kanala Platform in Greece (Grötsch *et al.*, 1998). Furthermore, terrigenous run-off during the OAE may have increased because of higher rainfall in the hinterland. Palynofacies studied in the Selli Level in Cismon have indicated a warm climate during black-shale formation, and a shift to cooler conditions afterwards (Hochuli *et al.*, 1999). Cooling during the mid-Aptian and at the Aptian/Albian boundary is also indicated by ammonoid population shifts in the Helvetic realm (Föllmi, 1989).

Changes in water circulation, temperature, nutrient content, oxygenation and pCO_2 led to floral and faunal changes and turnovers. The diversity of planktonic foraminifera at Roter Sattel is relatively low below the first black-shale interval. During deposition of the black shales of OAE 1a, acid bottom waters led to significant dissolution of the carbonate tests. Those that are preserved display modifications in size and thickness of their tests and in number and development of their chambers, and they changed their living strategies (Caron, 1983; Cobianchi *et al.*, 1999). With increasingly oligotrophic surface waters and less acid bottom waters, a slow speciation limited to simple forms was restored. Nannoconids are still present in the first black-shale interval at Roter Sattel but considerably reduced in number. This corresponds to the nannoconid crisis (Erba, 1994; Aguado *et al.*, 1999). Radiolarians have not been analysed in detail at Roter Sattel, but Erbacher & Thurow (1997) and Premoli Silva & Sliter (1999) stated that they underwent extinction/radiation events that were related to OAEs.

The second black-shale interval at Roter Sattel encompasses the *H. planispira*, *T. primula*, and *B. breggiensis* zones (Figure 3e). Organic matter and microfacies indicate a relatively shallow and/or proximal depositional environment (see section 5.5). While Larson *et al.* (1993) and Erbacher *et al.* (1999) placed the OAE 1b in the *H. planispira* Zone and correlated it with the Paquier level in the Vocontian Basin (Bréhéret, 1988), Erbacher & Thurow (1997) found a black shale in Umbria-Marche that is situated in the *T. primula* Zone. Still in Umbria-Marche, Coccioni *et al.* (1990) described a prominent black-shale interval in the *H. planispira* Zone (Monte Nerone level) and a thinner one in the *T. primula* Zone (Urbino level). At Roter Sattel as well as in the Umbria-Marche Basin, no major carbon-isotope shift is detectable around the beds representing OAE 1b (Erbacher & Thurow, 1997). In the Vocontian Basin, however, a black shale associated with an isotope shift is present

in the *T. bejaouaensis* Zone (Jacob level), and the Paquier level has also revealed rapid carbon-isotope shifts (Weissert & Bréhéret, 1991). In the western North Atlantic, a negative $\delta^{13}C$ shift of 0.5‰ marks the base of the black-shale interval (Erbacher *et al.*, 1999). It appears that the creation of OAE 1b was ruled by a sea-level rise that mobilized nutrients, and by anoxia confined to local and regional basins, rather than by dramatic global changes in carbon cycling such as occurred during OAE 1a. At Roter Sattel, eutrophication through continental run-off of nutrients and water stratification with anoxic intermediate and deep water led to the disappearance of complex foraminifer species within the genera *Ticinella* and *Globigerinelloides*. Simpler species survived in the shallow water column but have been only partly recorded because of dissolution of their tests by acid bottom waters.

As for OAE 1b, the black-shale intervals attributed to OAEs 1c and 1d do not show significant changes in the $\delta^{13}C$ curve (Figure 8; Erbacher & Thurow, 1997). At Roter Sattel, the equivalent of OAE 1c is within the second black-shale interval (Figure 3e). Benthic foraminifera and detrital quartz still indicate relatively shallow and proximal conditions, and reworked calpionellids point to erosion of pre-existing hemipelagic sediment. OAE 1d, situated in the *R. appenninica* Zone (Erbacher & Thurow, 1997; Erbacher *et al.*, 1999), may be indicated by the slightly elevated TOC at Roter Sattel (Figure 3f). In contrast to the other anoxic events, the planktonic foraminifera at Roter Sattel were not affected during OAEs 1c and 1d, suggesting that oligotrophic conditions prevailed. Their sizes and diversity increase from the *B. breggiensis* to the *R. appenninica* zones, reflecting the rapid evolution characterizing the Albian/Cenomanian boundary (Caron, 1983).

The third black-shale interval at Roter Sattel appears at the Cenomanian/Turonian boundary in the *W. archaeocretacea* Zone and is associated with OAE 2 (e.g., Arthur *et al.*, 1988; Farrimond *et al.*, 1990). It correlates with, for example, the Bonarelli Level in Italy (e.g., Arthur & Premoli Silva, 1982; Marcucci Passerini *et al.*, 1991; Luciani & Cobianchi, 1999), the Bahloul Formation in Tunisia (e.g., Caron *et al.*, 1999), and the Plenus and Meads marls in Sussex, UK (Gale *et al.*, 1993; Paul *et al.*, 1999). This interval is interpreted as corresponding to maximum-flooding and condensed deposits. Quartz grains indicate that a terrigenous source area was mobilized, and the sterane composition of the organic matter points to higher plants (Gjermeni, 1999). When compared to the previous black shales, there are no more reworked calpionellids, implying that the erosion potential of pre-existing hemipelagic sediment was diminished. Sea level reached its highest stand at around the Cenomanian/Turonian boundary (Haq *et al.*, 1987), and drowning of platforms occurred in several areas (e.g., in Morocco: Charrière *et al.*, 1997). A positive carbon-isotope shift is manifested at Roter Sattel (Figure 3h) and world-wide (see references above), and a chain of feed-back mechanisms triggered by oceanic plateau volcanism, as for the OAE 1a, can be suggested as the reason for this (Kerr, 1998). The record of the planktonic foraminifera at Roter Sattel reflects well this major event: rapid disappearance of complex species owing to eutrophication and oxygen-deficient water, which affected their life cycle (e.g., *Rotalipora*), and formation of anoxic and acid bottom waters, which led to dissolution of the simpler and opportunistic species that still lived in the surface water (e.g., *Hedbergella, Whiteinella*). Recovery was slow, as indicated by the delayed appearance of *H. helvetica*.

It is not the purpose of this paper to discuss the various and complex mechanisms leading to black-shale formation. At Roter Sattel, however, it appears that each black-shale unit has its own characteristics, and that different factors were responsible for their formation or the same factors but in different proportions. When compared to time-equivalent deposits in other areas, it is seen that global signals are generally well recorded, but that local factors, such as basin configuration resulting from differential subsidence, water circulation depending on opening and closing of gateways, availability of terrigenous source areas, and climate depending on palaeolatitude, were also important and partially distorted the global signal.

The deposits in between the black-shale intervals are equally diverse. Periods dominated by (most probably) climatically controlled formation of limestone-marl couplets alternated with periods when currents winnowed the ocean floor. Some intervals displaying channelling and gravity flows suggest slope instabilities, whereas in other intervals sediment accumulated without any disturbance. These variations can be explained by a combination of parameters such as sea-level changes that forced sediment to prograde or retrograde and partly controlled planktonic productivity and water circulation, tectonic movements that shaped basin morphology and opened or closed gateways for ocean currents, and climate changes that modulated the input of siliciclastics and nutrients.

7. Conclusions

The well-exposed section of Aptian–Lower Turonian hemipelagic sediments at Roter Sattel has provided

the opportunity to study the record of mid-Cretaceous oceanographic changes in great detail. The biostratigraphic framework based on planktonic foraminifera has allowed the calibration of the depositional sequences and the three major black-shale intervals. Sequence boundaries, transgressive surfaces, and maximum-flooding events comparable to those observed elsewhere in European basins have been recorded despite local and regional tectonic activity, implying that sea-level fluctuations were important in generating these sequences. The black-shale intervals seen at Roter Sattel can be correlated with the OAEs 1a (first interval), 1b, 1c and 1d (second interval), and 2 (third interval). The marked positive $\delta^{13}C$ shifts in the first and third interval correspond well with the signal observed on a global scale. Regional climate and terrigenous run-off controlling nutrient availability and organic productivity, and regional tectonic activity shaping basin morphology and modifying oceanic currents were important factors that led to the sedimentary record now preserved. However, global signals such as eustatic sea-level changes and fluctuations in the carbon cycle are recognizable, even if they may have been distorted or attenuated.

Acknowledgements

This study is part of project No. 20-39257.93 of the Swiss National Science Foundation, whose financial support is gratefully acknowledged. The isotope analyses were carried out at the ETH Zurich, and we thank H. Weissert and A. P. Menegatti for their help. We also thank P. Hochuli and L. Braillard who assisted with the interpretation of the palynofacies, and S. Dall'Agnolo who assembled the photographs and critically read a first version of the manuscript. The helpful comments and suggestions by R. Gaupp, H. von Eynatten, and an anonymous reviewer are greatly appreciated. We also thank D. J. Batten for his careful editing of the manuscript.

References

Aguado, R., Castro, J. M., Company, M. & de Gea, G. A. 1999. Aptian bio-events – an integrated biostratigraphic analysis of the Almadich Formation, inner Prebetic domain, SE Spain. *Cretaceous Research* **20**, 663–683.

Arthur, M. A., Dean, W. E. & Pratt, L. M. 1988. Geochemical and climatic effects of increased marine organic carbon burial at the Cenomanian/Turonian boundary. *Nature* **335**, 714–717.

Arthur, M. A. & Premoli Silva, I. 1982. Development of widespread organic carbon-rich strata in the Mediterranean Tethys. In *Nature and origin of Cretaceous carbon-rich facies* (eds Schlanger, S. O. & Cita, M. B.), pp. 6–52 (Academic Press, London).

Baud, A. & Septfontaine, M. 1980. Présentation d'un profil palinspastique de la nappe des Préalpes médianes en Suisse occidentale. *Eclogae Geologicae Helvetiae* **73**, 651–660.

Baudin, F., Fiet, N., Coccioni, R. & Galeotti, S. 1998. Organic matter characterisation of the Selli Level (Umbria-Marche Basin, central Italy). *Cretaceous Research* **19**, 701–714.

Berger, A., Loutre, M. F. & Dehant, V. 1989. Astronomical frequencies for pre-Quaternary palaeoclimate studies. *Terra Nova* **1**, 474–479.

Bralower, T. J., Arthur, M. A., Leckie, R. M., Sliter, W. V., Allard, D. J. & Schlanger, S. O. 1994. Timing and paleoceanography of oceanic dysoxia/anoxia in the Late Barremian to Early Aptian (Early Cretaceous). *Palaios* **9**, 335–369.

Bralower, T. J., Fullagar, P. D., Paull, C. K., Dwyer, G. S. & Leckie, R. M. 1997. Mid-Cretaceous strontium-isotope stratigraphy for deep-sea sections. *Geological Society of America, Bulletin* **109**, 1421–1442.

Bréhéret, J. G. 1988. Episodes de sédimentation riche en matière organique dans les marnes bleues d'âge aptien et albien de la partie pélagique du bassin vocontien. *Bulletin de la Société Géologique de France* (*8*) **4**, 349–356.

Caron, C. 1973. Survol géologique des Alpes occidentales. *Bulletin de la Société Fribourgeoise des Sciences Naturelles* **62**, 73–81.

Caron, M. 1983. La spéciation chez les foraminifères planctoniques: une réponse adaptée aux contraintes de l'environnement. *Zitteliana* **10**, 671–676.

Caron, M., Robaszynski, F., Amedro, F., Baudin, F., Deconinck, J.-F., Hochuli, P., Von Salis-Perch Nielsen, K. & Tribovillard, N. 1999. Estimation de la durée de l'événement anoxique global au passage Cénomanien/Turonien. Approche cyclostratigraphique dans la formation Bahloul en Tunisie centrale. *Bulletin de la Société Géologique de France* **170**, 145–160.

Charrière, A., Andreu, B., Ciszak, R., Kennedy, W. J., Rossi, A. & Vila, J.-M. 1997. La transgression du Cénomanien supérieur dans la Haute Moulouya et le Moyen Atlas méridional, Maroc. *Geobios* **31**, 551–569.

Cobianchi, M., Luciani, V. & Menegatti, A. 1999. The Selli level of the Gargano promontory, Apulia, southern Italy: foraminiferal and calcareous nannofossil data. *Cretaceous Research* **20**, 255–269.

Coccioni, R., Franchi, R., Nesci, O., Perilli, N., Wezel, F.-C. & Battistini, F. 1990. Stratigrafia, micropaleontologia e mineralogia delle Marne a Fucoidi (Aptiano inferiore–Albiano superiore) delle sezioni di Poggio le Guaine e del Fiume Bosso (Appennino umbro-marchigiano). *Atti II Convegno Internazionale Fossili, Evoluzione, Ambiente*, Pergola, 1987, 163–201.

Coccioni, R., Erba, E. & Premoli Silva, I. 1992. Barremian–Aptian calcareous plankton biostratigraphy from the Gorgo Cerbera section (Marche, central Italy) and implications for plankton evolution. *Cretaceous Research* **13**, 517–537.

Dall'Agnolo, S. 2000. Le Crétacé de la Nappe de la Brèche (Préalpes franco-suisses). Données nouvelles et essai de synthèse stratigraphique et paléogéographique. *Eclogae Geologicae Helvetiae* **93**, 157–174.

D'Argenio, B., Ferreri, V., Ardillo, F. & Buonocunto, F. P. 1993. Microstratigrafia e stratigrafia sequenziale. Studi sui depositi di piattaforma carbonatica nel Cretacico del Monte Maggiore (Appennino Meridionale). *Bollettino della Società Geologica Italiana* **112**, 739–749.

De Wever, P., Azéma, J. & Fourcade, E. 1994. Radiolaires et radiolarites: production primaire, diagenèse et paléogéographie. *Bulletin des Centres de Recherches Exploration-Production Elf Aquitaine* **18**, 315–379.

Dunbar, G. B., Dickens, G. R. & Carter, R. M. 2000. Sediment flux across the Great Barrier Reef Shelf to the Queensland Trough over the last 300 ky. *Sedimentary Geology* **133**, 49–92.

Einsele, G. & Ricken, W. 1991. Limestone-marl alternations – an overview. In *Cycles and events in stratigraphy* (eds Einsele, G., Ricken, W. & Seilacher, A.), pp. 23–47 (Springer-Verlag, Berlin).

Erba, E. 1994. Nannofossils and superplumes: the early Aptian "nannoconid crisis". *Paleoceanography* **9**, 483–501.

Erba, E., Castradori, D., Guasti, G. & Ripepe, M. 1992. Calcareous nannofossils and Milankovitch cycles: the example of the Albian Gault Clay Formation (southern England). *Palaeogeography, Palaeoclimatology, Palaeoecology* **93**, 47–69.

Erba, E., Channell, J. E. T., Claps, M., Jones, C., Larson, R., Opdyke, B., Premoli Silva, I., Riva, A., Salvini, G. & Torricelli, S. 1999. Integrated stratigraphy of the Cismon Apticore (southern Alps, Italy): a "reference section" for the Barremian–Aptian interval at low latitudes. *Journal of Foraminiferal Research* **29**, 371–391.

Erbacher, J. & Thurow, J. 1997. Influence of oceanic anoxic events on the evolution of mid-Cretaceous radiolaria in the North Atlantic and western Tethys. *Marine Micropaleontology* **30**, 139–158.

Erbacher, J., Hemleben, C., Huber, B. T. & Markey, M. 1999. Correlating environmental changes during early Albian oceanic anoxic event 1B using benthic foraminiferal paleoecology. *Marine Micropaleontology* **38**, 7–28.

Espitalié, J., Deroo, G. & Marquis, F. 1985. La pyrolyse Rock-Eval et ses applications. *Revue de l'Institut Français du Pétrole* **40**, 563–579.

Farrimond, P., Eglinton, G., Brassell, S. C. & Jenkyns, H. C. 1990. The Cenomanian/Turonian anoxic event in Europe: an organic geochemical study. *Marine and Petroleum Geology* **7**, 75–89.

Föllmi, K. B. 1989. Evolution of the Mid-Cretaceous triad. *Lecture Notes in Earth Sciences* **23**, 153 pp. (Springer-Verlag, Berlin).

Föllmi, K. B., Weissert, H., Bisping, M. & Funk, H. 1994. Phosphogenesis, carbon-isotope stratigraphy, and carbonate-platform evolution along the Lower Cretaceous northern Tethyan margin. *Geological Society of America, Bulletin* **106**, 729–746.

Gale, A. S., Jenkyns, H. C., Kennedy, W. J. & Corfield, R. M. 1993. Chemostratigraphy versus biostratigraphy: data from around the Cenomanian-Turonian boundary. *Journal of the Geological Society, London* **150**, 29–32.

Gjermeni, M. 1999. *La signification environnementale de la matière organique sédimentaire: exemple des faciès pélagiques de l'Aptien, de l'Albien et du Cénomanien des Préalpes Médianes Romandes* (*Suisse*). PhD Thesis, University of Fribourg, Switzerland, 183 pp. [Unpublished]

Gradstein, F. M., Agterberg, F. P., Ogg, J. G., Hardenbol, J., van Veen, P., Thierry, J. & Huang, Z. 1995. A Triassic, Jurassic and Cretaceous time scale. In *Geochronology, time scales and global stratigraphic correlation* (eds Berggren, W. A., Kent, D. V., Aubry, M. P. & Hardenbol, J.), *SEPM* (*Society for Sedimentary Geology*), *Special Publication* **54**, 95–126.

Gröcke, D. R., Hesselbo, S. P. & Jenkyns, H. C. 1999. Carbon-isotope composition of Lower Cretaceous fossil wood: ocean-atmosphere chemistry and relation to sea-level change. *Geology* **27**, 155–158.

Grötsch, J., Billing, I. & Vahrenkamp, V. 1998. Carbon-isotope stratigraphy in shallow-water carbonates: implications for Cretaceous black-shale deposition. *Sedimentology* **45**, 623–634.

Hable, R. 1997. *Biostratigraphie, Sedimentologie und paläogeographische Entwicklung der Préalpes Médianes des Chablais* (*Haute Savoie*) *vom Apt bis Unter-Eozän*. PhD Thesis, University of Fribourg, Switzerland, 324 pp. [Unpublished]

Haq, B. U., Hardenbol, J. & Vail, P. R. 1987. Chronology of fluctuating sea levels since the Triassic. *Science* **235**, 1156–1167.

Hardenbol, J., Thierry, J., Farley, M. B., Jacquin, T., de Graciansky, P.-C. & Vail, P. R. 1998. Cretaceous sequence chronostratigraphy. In *Mesozoic and Cenozoic sequence stratigraphy of European basins* (eds de Graciansky, P.-C., Hardenbol, J., Jacquin, T. & Vail, P. R.), *SEPM* (*Society for Sedimentary Geology*), *Special Publication* **60** (chart).

Hochuli, P. A., Menegatti, A. P., Weissert, H., Riva, A., Erba, E. & Premoli Silva, I. 1999. Episodes of high productivity and cooling in the early Aptian Alpine Tethys. *Geology* **27**, 657–660.

Hochuli, P. A. & Strasser, A. 2000. Sequence-stratigraphic expression of major environmental changes in the Early Aptian of the Western Tethys. *Abstracts, AAPG Annual Convention, New Orleans*, A68.

Huang, W. Y. & Meinschein, W. G. 1979. Sterols as ecological indicators. *Geochimica Cosmochimica Acta* **43**, 739–745.

Hunt, D. & Tucker, M. E. 1993. Sequence stratigraphy of carbonate shelves with an example from the mid-Cretaceous (Urgonian) of southeast France. In *Sequence stratigraphy and facies associations* (eds Posamentier, H. W., Summerhayes, C. P., Haq, B. U. & Allen, G. P.), *International Association of Sedimentologists, Special Publication* **18**, 307–341.

Jenkyns, H. C. 1980. Cretaceous anoxic events: from continents to oceans. *Journal of the Geological Society, London* **137**, 171–188.

Jenkyns, H. C. 1995. Carbon isotope stratigraphy and paleoceanographic significance of the Lower Cretaceous shallow-water carbonates of Resolution Guyot, Mid-Pacific Mountains. In *Proceedings of the Ocean Drilling Program, Scientific Results* (eds Winterer, E. L., Sager, W. W. & Firth, J. V.), **143**, 99–104.

Jenkyns, H. C. & Clayton, C. J. 1986. Black shales and carbon isotopes in pelagic sediments from the Tethyan Lower Jurassic. *Sedimentology* **33**, 87–106.

Jordan, D. W. 1985. Trace fossils and depositional environments of Upper Devonian black shales, east-central Kentucky, U.S.A. In *Biogenic structures: their use in interpreting depositional environments* (ed. Curran, H. A.), *SEPM* (*Society for Sedimentary Geology*), *Special Publication* **35**, 279–298.

Kerr, A. C. 1998. Oceanic plateau formation: a cause of mass extinction and black shale deposition around the Cenomanian-Turonian boundary? *Journal of the Geological Society, London* **155**, 619–626.

Larson, R. L. 1991. Geological consequences of superplumes. *Geology* **19**, 963–966.

Larson, R. L. & Erba, E. 1999. Onset of the mid-Cretaceous greenhouse in the Barremian–Aptian: igneous events and the biological, sedimentary, and geochemical responses. *Paleoceanography* **14**, 663–678.

Larson, R. L., Fischer, A. G., Erba, E. & Premoli Silva, I. (eds) 1993. *Apticore-Albicore; a workshop report on global events and rhythms of the Mid-Cretaceous*, 4–9 October 1992, Perugia, Italy, 56 pp.

Loutit, T. S., Hardenbol, J., Vail, P. R. & Baum, G. R. 1988. Condensed sections: the key to age determination and correlation of continental margin sequences. In *Sea-level changes: an integrated approach* (eds Wilgus, C. K., Hastings, B. S., Kendall, C. G. St. C., Posamentier, H. W., Ross, C. A. & Van Wagoner, J. C.), *SEPM* (*Society for Sedimentary Geology*), *Special Publication* **42**, 183–213.

Luciani, V. & Cobianchi, M. 1999. The Bonarelli Level and other black shales in the Cenomanian–Turonian of the northeastern Dolomites (Italy): calcareous nannofossils and foraminiferal data. *Cretaceous Research* **20**, 135–167.

Marcucci Passerini, M., Bettini, P., Dainelli, J. & Sirugo, A. 1991. The "Bonarelli Horizon" in the Central Apennines (Italy): radiolarian biostratigraphy. *Cretaceous Research* **12**, 321–331.

Mattioli, E. 1997. Nannoplankton productivity and diagenesis in the rhythmically bedded Toarcian–Aalenian Fiuminata section (Umbria-Marche Apennine, central Italy). *Palaeogeography, Palaeoclimatology, Palaeoecology* **130**, 113–133.

Menegatti, A. P., Weissert, H., Brown, R. S., Tyson, R. V., Farrimond, P., Strasser, A. & Caron, M. 1998. High-resolution $\delta^{13}C$ stratigraphy through the early Aptian "Livello Selli" of the Alpine Tethys. *Paleoceanography* **13**, 530–545.

Mettraux, M. & Mosar, J. 1989. Tectonique alpine et paléotectonique liasique dans les Préalpes Médianes en rive droite du Rhône. *Eclogae Geologicae Helvetiae* **82**, 517–540.

Milliman, J. D. & Droxler, A. W. 1996. Neritic and pelagic carbonate sedimentation in the marine environment: ignorance is not bliss. *Geologische Rundschau* **85**, 496–504.

Milliman, J. D., Freile, D., Steinen, R. P. & Wilber, R. J. 1993. Great Bahama Bank aragonitic muds: mostly inorganically precipitated, mostly exported. *Journal of Sedimentary Petrology* **63**, 589–595.

Morel, L. 1998. *Stratigraphie à haute résolution du passage Cénomanien–Turonien*. PhD thesis, Université Paris VI, France, 223 pp. [Unpublished]

Page, C. 1969. Observations géologiques sur les Préalpes au NW des Gastlosen orientales. *Bulletin de la Société Fribourgeoise des Sciences Naturelles* **58**, 79–180.

Pasquier, J.-B. & Strasser, A. 1997. Platform-to-basin correlation by high-resolution sequence stratigraphy and cyclostratigraphy (Berriasian, Switzerland and France). *Sedimentology* **44**, 1071–1092.

Paul, C. R. C., Lamolda, M. A., Mitchell, S. F., Vaziri, M. R., Gorostidi, A. & Marshall, J. D. 1999. The Cenomanian-Turonian boundary at Eastbourne (Sussex, UK): a proposed European reference section. *Palaeogeography, Palaeoclimatology, Palaeoecology* **150**, 83–121.

Premoli Silva, I. & Sliter, W. V. 1994. Cretaceous planktonic foraminiferal biostratigraphy and evolutionary trends from the Bottaccione section, Gubbio, Italy. *Palaeontographica Italica* **82**, 1–89.

Premoli Silva, I. & Sliter, W. V. 1999. Cretaceous paleoceanography: evidence from planktonic foraminiferal evolution. In *Evolution of the Cretaceous ocean-climate system* (eds Barrera, E. & Johnson, C. C.). *Geological Society of America, Special Paper* **332**, 301–328.

Premoli Silva, I., Erba, E., Salvini, G., Locatelli, C. & Verga, D. 1999. Biotic changes in Cretaceous oceanic anoxic events of the Tethys. *Journal of Foraminiferal Research* **29**, 352–370.

Python-Dupasquier, C. 1990. *La formation de l'Intyamon* ("*Crétacé moyen*") *des Préalpes Médianes Romandes*. PhD Thesis, University of Fribourg, Switzerland, 197 pp. [Unpublished]

Ricken, W. & Eder, W. 1991. Diagenetic modification of calcareous beds – an overview. In *Cycles and events in stratigraphy* (eds Einsele, G., Ricken, W. & Seilacher, A.), pp. 430–449 (Springer-Verlag, Berlin).

Robaszynski, F. & Caron, M. 1995. Foraminifères planctoniques du Crétacé: commentaire de la zonation Europe-Méditerranée. *Bulletin de la Société Géologique de France* **166**, 681–692.

Robaszynski, F., Caron, M., Dupuis, C., Amédro, F., González Donoso, J.-M., Linares, D., Hardenbol, J., Gartner, S., Calandra, F. & Deloffre, R. 1990. A tentative integrated stratigraphy in the Turonian of central Tunisia: formations, zones and sequential stratigraphy in the Kalaat Senan area. *Bulletin des Centres de Recherches Exploration-Production Elf Aquitaine* **14**, 213–384.

Röhl, U. & Ogg, J. G. 1996. Aptian–Albian sea level history from guyots in the western Pacific. *Paleoceanography* **11**, 595–624.

Schlanger, S. O. & Jenkyns, H. C. 1976. Cretaceous oceanic anoxic events: causes and consequences. *Geologie en Mijnbouw* **55**, 179–184.

Scholle, P. A., Arthur, M. A. & Ekdale, A. A. 1983. Pelagic environment. In *Carbonate depositional environments* (eds Scholle, P. A., Bebout, D. G. & Moore, C. H.). *American Association of Petroleum Geologists, Memoir* **33**, 619–691.

Stampfli, G. M. 1993. Le Briançonnais, terrain exotique dans les Alpes? *Eclogae Geologicae Helvetiae* **86**, 1–45.

Steffen, D. & Gorin, G. 1993. Palynofacies of the Upper Tithonian–Berriasian deep-sea carbonates in the Vocontian Trough (SE France). *Bulletin des Centres de Recherches Exploration-Production Elf Aquitaine* **17**, 235–247.

Stow, D. A. V. 1994. Deep sea processes of sediment transport and deposition. In *Sediment transport and depositional processes* (ed. Pye, K.), pp. 257–291 (Blackwell, Oxford).

Strasser, A., Pittet, B., Hillgärtner, H. & Pasquier, J.-B. 1999. Depositional sequences in shallow carbonate-dominated sedimentary systems: concepts for a high-resolution analysis. *Sedimentary Geology* **128**, 201–221.

Strohmenger, C. & Strasser, A. 1993. Eustatic controls on the depositional evolution of Upper Tithonian and Berriasian deep-water carbonates (Vocontian Trough, SE France). *Bulletin des Centres de Recherches Exploration-Production Elf Aquitaine* **17**, 183–203.

Tarduno, J. A., Sliter, W. V., Kroenke, L., Leckie, M., Mayer, H., Mahoney, J. J., Musgrave, R., Storey, M. & Winterer, E. L. 1991. Rapid formation of the Ontong Java Plateau by Aptian mantle plume volcanism. *Science* **18**, 399–403.

Terrab, S. 1996. Le Cénomanien–Turonien d'Agadir. Stratigraphie et diagenèse (nodulisation). *Ecole des Mines de Paris, Mémoires des Sciences de la Terre* **27**, 254 pp.

Trümpy, R. 1980. *Geology of Switzerland – a guide book. Part A: an outline of the geology of Switzerland*, 104 pp. (Wepf & Co., Basel, New York).

Vail, P. R., Audemard, F., Bowman, S. A., Eisner, P. N. & Perez-Cruz, C. 1991. The stratigraphic signatures of tectonics, eustasy and sedimentology – an overview. In *Cycles and events in stratigraphy* (eds Einsele, G., Ricken, W. & Seilacher, A.), pp. 617–659 (Springer-Verlag, Berlin).

Weissert, H. & Bréhéret, J.-G. 1991. A carbonate carbon-isotope record from Aptian–Albian sediments of the Vocontian Trough (SE France). *Bulletin de la Société Géologique de France* **162**, 1133–1140.

Weissert, H. & Mohr, H. 1996. Late Jurassic climate and its impact on carbon cycling. *Palaeogeography, Palaeoclimatology, Palaeoecology* **122**, 27–43.